Role of carbon allocation efficiency in the temperature dependence of autotroph growth rates

Bernardo García-Carreras[a,1,2], Sofía Sal[a], Daniel Padfield[b], Dimitrios-Georgios Kontopoulos[a], Elvire Bestion[b], C.-Elisa Schaum[b,3], Gabriel Yvon-Durocher[b], and Samrāt Pawar[a,2]

[a]Department of Life Sciences, Imperial College London, Ascot, Berkshire, SL5 7PY, United Kingdom; and [b]Environment and Sustainability Institute, University of Exeter, Penryn, Cornwall, TR10 9EZ, United Kingdom

Edited by William H. Schlesinger, Earth and Ocean Sciences, Nicholas School of the Environment, Duke University, Durham, NC, and approved June 15, 2018 (received for review January 5, 2018)

Relating the temperature dependence of photosynthetic biomass production to underlying metabolic rates in autotrophs is crucial for predicting the effects of climatic temperature fluctuations on the carbon balance of ecosystems. We present a mathematical model that links thermal performance curves (TPCs) of photosynthesis, respiration, and carbon allocation efficiency to the exponential growth rate of a population of photosynthetic autotroph cells. Using experiments with the green alga, *Chlorella vulgaris*, we apply the model to show that the temperature dependence of carbon allocation efficiency is key to understanding responses of growth rates to warming at both ecological and longer-term evolutionary timescales. Finally, we assemble a dataset of multiple terrestrial and aquatic autotroph species to show that the effects of temperature-dependent carbon allocation efficiency on potential growth rate TPCs are expected to be consistent across taxa. In particular, both the thermal sensitivity and the optimal temperature of growth rates are expected to change significantly due to temperature dependence of carbon allocation efficiency alone. Our study provides a foundation for understanding how the temperature dependence of carbon allocation determines how population growth rates respond to temperature.

growth rate | allocation efficiency | temperature dependence | autotrophs | carbon flux

All autotroph cells show a strong dependence of doubling rate on environmental temperature (1–3). This doubling rate drives exponential population growth rate in unicellular autotrophs and somatic growth in multicellular autotrophs, and is often used as a measure of fitness (4, 5). Global primary productivity depends fundamentally on the growth rates of photosynthetic tissue in aquatic and terrestrial photo-autotrophs—mostly phytoplankton and terrestrial plants, respectively (6, 7). Therefore, understanding the mechanistic, physiological basis of temperature-dependent exponential growth rate in autotroph cell populations is of fundamental importance. In particular, ongoing climate change will not only alter mean temperatures, but also likely exacerbate the thermal variability faced by autotrophs in the future (8, 9), meaning that more populations will be challenged with novel environments in which to compete and persist. In these situations, fitness can be primarily driven by the exponential growth rate of cells, either at low cell densities (e.g., competitive fitness among phytoplankton) or during somatic growth (e.g., germination or phenological change in terrestrial plants) (10, 11).

The mechanistic basis for the intraspecific temperature dependence of growth rates in photosynthetic tissue requires an understanding of a number of underlying metabolic processes, especially photosynthesis and respiration. The cell fixes carbon through photosynthesis, and part of that intracellular carbon is used in respiration to generate the carbon skeleton as well as usable forms of energy essential for maintenance and growth (12–15). The temperature dependencies of these metabolic processes take the form of unimodal thermal performance curves (TPCs), with an exponential increase of the rate followed by a sharp decline at higher temperatures (Fig. 1*A*) (16, 17). Current knowledge suggests that the photosynthesis and respiration TPCs differ, partly because temperature affects their underlying metabolic reactions differently (2, 3, 18, 19). The carbon potentially available for growth is expected to be proportional to the difference between these two metabolic rates (net carbon flux; solid line in Fig. 1*F*), and therefore differences in the TPCs of these processes should influence the shape of the emergent growth rate TPC (*SI Appendix*, section S3) (3, 20).

Not all available carbon in the cell, however, is used in growth (2, 3, 20, 21). This allocation to growth, typically quantified as an efficiency, could be expected to depend on a range of environmental variables, especially temperature, CO_2 concentration (22), and, in terrestrial plants, water availability or movement of photosynthates out of the cell (23). The temperature dependence of carbon allocation efficiency has received little attention and has rarely been considered in population growth models (14, 19, 24), but may also be a significant factor influencing the growth TPC. Here, we develop a mathematical model for the contribution of the TPCs of photosynthesis,

Significance

To predict how plant growth rate will respond to temperature requires understanding how temperature drives the underlying metabolic rates. Although past studies have considered the temperature dependences of photosynthesis and respiration rates underlying growth, they have largely overlooked the temperature dependence of carbon allocation efficiency. By combining a mathematical model that links exponential growth rate of a population of photosynthetic cells to photosynthesis, respiration, and carbon allocation; to an experiment on a freshwater alga; and to a database covering a wide range of taxa, we show that allocation efficiency is crucial for predicting how growth rates will respond to temperature change across aquatic and terrestrial autotrophs, at both short and long (evolutionary) timescales.

Author contributions: B.G.-C., G.Y.-D., and S.P. designed research; B.G.-C. and S.P. performed research; B.G.-C., S.S., D.P., and D.-G.K. analyzed data; and B.G.-C., S.S., E.B., C.-E.S., G.Y.-D., and S.P. wrote the paper.

The authors declare no conflict of interest.

This article is a PNAS Direct Submission.

[1]Present address: Department of Biology, University of Florida, Gainesville, FL 32611.

[2]To whom correspondence may be addressed. Email: bgarciacarreras@gmail.com or s.pawar@imperial.ac.uk.

[3]Present address: Institut für marine Ökosystem- und Fischereiwissenschaften, Universität Hamburg, 20148 Hamburg, Germany.

This article contains supporting information online at www.pnas.org/lookup/suppl/doi:10.1073/pnas.1800222115/-/DCSupplemental.

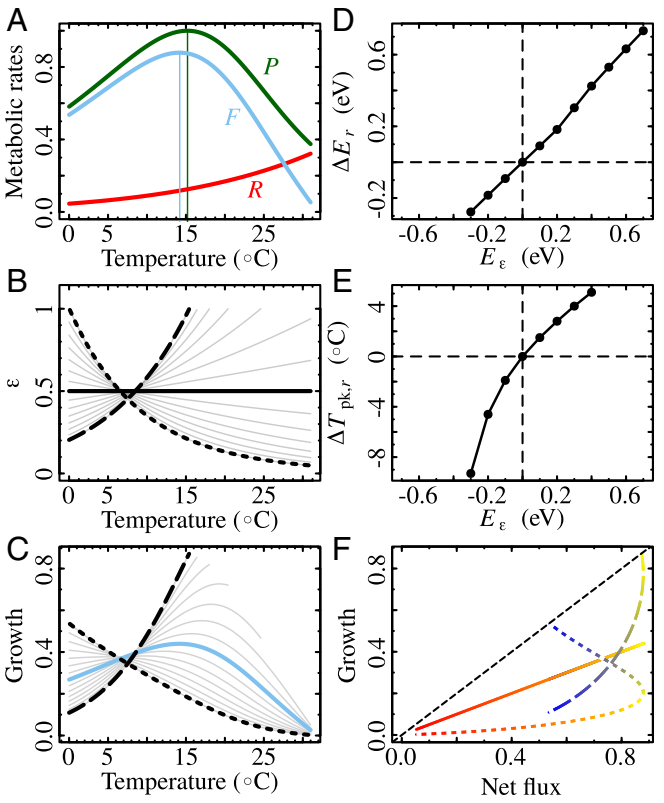

Fig. 1. The impact of a temperature-dependent allocation efficiency $\varepsilon(T)$ on the TPC of growth rates in a population of photosynthetic cells. (*A*) Real TPCs for photosynthesis *P*, respiration *R*, and resulting net flux *F* for *Cladophora glomerata* (a green alga). (*B*) Allocation efficiency $\varepsilon(T)$ expressed as a Boltzmann–Arrhenius function (Eq. **4** and *SI Appendix*, section S1.2) with a range of different temperature dependences (set by the activation energy E_ε). (*C*) The result is a range of different potential growth TPCs. (*D* and *E*) ΔE_r (Eq. **5**) (*D*) and $\Delta T_{\mathrm{pk},r}$ (Eq. **6**) (*E*) as functions of the temperature dependence of $\varepsilon(T)$. (*F*) Relationships between potential growth and net flux (blues represent colder and reds warmer temperatures). A temperature-dependent $\varepsilon(T)$ affects the shape of the growth TPC and as a result how growth responds to temperature. The growth–net flux relationship can be highly nonlinear in this scenario, with the direction of the nonlinearity (blue-to-red trajectory) depending upon whether $\varepsilon(T)$ increases or decreases with T (*B*). Temperature-independent $\varepsilon(\kappa)$ (solid black line in *B*) produces growth TPCs that are qualitatively equal to those of net flux (solid blue line in *C*) and that are unaffected by $\varepsilon(T)$. In *B*, *C*, and *F* the dotted lines are for $E_\varepsilon = -0.7$ and the dashed lines are for $E_\varepsilon = 0.7$. Note that in *D* and *E*, larger values of $|E_\varepsilon|$ produce curves that do not peak within the experimental temperature range (*C*).

respiration, and carbon allocation efficiency to the temperature dependence of doubling rate of a population of photosynthetic autotroph cells. In particular, we focus on the effect of temperature-dependent carbon allocation efficiency on two key parameters of growth rate TPCs: thermal sensitivity (activation energy, E; Fig. 1) and optimal temperature (T_{pk}). These two parameters strongly determine the temperature dependence of fitness of populations in their operational, ecologically relevant temperature range and have been extensively used in metabolic theories in ecology (*SI Appendix*, section S4) (25–27). We use laboratory experiments on the freshwater alga *Chlorella vulgaris*, combined with an analysis of data across a diversity of aquatic and terrestrial plants (38 species in 21 orders covering all major phyla), to quantify how much the temperature dependence of carbon allocation efficiency can affect growth rate TPCs.

Theory

Our model incorporates the TPCs of photosynthesis, respiration, and allocation efficiency into the TPC of doubling rate of a population of photosynthetic autotroph cells (for further details of the model, see *SI Appendix*, section S1). We begin with a single autotroph population's biomass density N (e.g., μg C/m^2 or m^3) in the exponential phase of growth, integrated over a 24-h period,

$$\frac{1}{N}\frac{\mathrm{d}N}{\mathrm{d}t} = r = \varepsilon F, \qquad [1]$$

where F is net carbon flux (1/d) and ε (dimensionless) is the allocation efficiency and captures the allocation of the fixed intracellular carbon to growth. Growth here accounts for both individual cell growth [e.g., through carbon storage (10, 28)] and population growth. While more complex models that mechanistically include intracellular processes are possible (28–33), the simplicity of our model allows comparisons with the type of experimental data that are typically feasible to collect (e.g., ref. 2). Net carbon flux F (henceforth "net flux") is a measure of mass-specific growth potential, given by

$$F = P - R, \qquad [2]$$

where P is net photosynthesis (difference between maximum gross photosynthetic rate in nutrient-saturated and optimal-light conditions and daytime respiration), and R is nighttime (dark) respiration. Thus, F (blue line in Fig. 1*A*) represents an upper bound for how much of the carbon fixed in photosynthesis could be available to the cells for growth, after accounting for respiratory and other losses. We fitted the model to laboratory experiments performed in nutrient-saturated conditions—we accordingly assume nutrient saturation. However, the model could be extended to include nutrient limitation (*SI Appendix*, section S1). We come back to the possible effects of nutrient limitation on growth rate TPCs in *Discussion*.

An allocation efficiency implies that some of the carbon assimilated is "lost" from the cells. This is to be expected. For example, phytoplankton cells commonly exude photosynthetic assimilates instead of storing them or using them for growth (34, 35), and that carbon then enters the broader carbon cycle (ref. 36 and *SI Appendix*, section S1.2). In higher plants, carbon may also be allocated away from leaves to nonphotosynthetic tissues; that carbon would no longer be available for growth of the focal population of photosynthetic cells.

We now specify the TPCs of each of the parameters of the growth model (Eq. **1**). For photosynthesis and respiration, we use the Schoolfield–Sharpe model without low-temperature inactivation (2, 3, 16):

$$B = \frac{B_0 \exp\left(-\frac{E}{k}\left(\frac{1}{T} - \frac{1}{T_{\mathrm{ref}}}\right)\right)}{1 + \exp\left(\frac{E_{\mathrm{D}}}{k}\left(\frac{1}{T_{\mathrm{h}}} - \frac{1}{T}\right)\right)}. \qquad [3]$$

Here, B is a metabolic rate (1/d) at a given temperature T (in kelvins), B_0 is approximately (37) the rate (1/d) at a reference temperature T_{ref}, E and E_{D} are the activation and deactivation energies (electronvolts) that set the relative rate of increase up to and decrease from the maximum, respectively, T_{h} is the temperature at which the rate is half inactive due to high temperatures, and $k \approx 8.617 \times 10^{-5}$ eV/K is the Boltzmann constant. Example P and R TPCs are shown in Fig. 1*A*. This model has been shown to fit well to photosynthesis and respiration rate data (2, 3, 16, 38, 39).

For the TPC of allocation efficiency, we use the Boltzmann–Arrhenius (BA) equation

$$\varepsilon = \varepsilon_0 \exp\left(-\frac{E_\varepsilon}{k}\left(\frac{1}{T}-\frac{1}{T_{\text{ref}}}\right)\right), \quad [4]$$

where normalization constant ε_0 is the efficiency at T_{ref}, and E_ε sets the relative rate of change of $\varepsilon(T)$ with T. There is limited evidence for the temperature dependence of ε over the operational temperature range of organisms (38, 40, 41); here we make no a priori assumption about the directionality of the temperature dependence and consider both positive and negative values of E_ε (Fig. 1*B*). The BA form for $\varepsilon(T)$ (Eq. **4**) allows us to study the effect of putative thermodynamic constraints on the metabolic rates underlying allocation and is also supported by our experimental data (see below). In *SI Appendix*, section S12 we show that using a more phenomenological quadratic TPC (*SI Appendix*, sections S1.2 and S6) for $\varepsilon(T)$ does not qualitatively change our results.

To quantify how a temperature-dependent $\varepsilon(T)$ alters the potential growth rate TPC we compare it to the assumption of a constant, temperature-independent $\varepsilon = \kappa$ [henceforth $\varepsilon(\kappa)$], by expressing changes in E_r (activation energy of growth rate) and $T_{\text{pk},r}$ (temperature of peak growth rate) as a result of the temperature dependence of ε; i.e.,

$$\Delta E_r = E_r(\varepsilon(T)) - E_r(\varepsilon(\kappa)) \quad [5]$$

$$\Delta T_{\text{pk},r} = T_{\text{pk},r}(\varepsilon(T)) - T_{\text{pk},r}(\varepsilon(\kappa)). \quad [6]$$

The effect of $\varepsilon(T)$ (Eq. **4**) on E_r is straightforward to derive analytically: $\Delta E_r = E_\varepsilon$ (Fig. 1*D* and *SI Appendix*, section S5). It is not possible to analytically derive the effect of $\varepsilon(T)$ on $T_{\text{pk},r}$. However, numerical simulations show that $\Delta T_{\text{pk},r}$ is expected to correlate positively with E_ε (Fig. 1*E*).

Substituting the TPCs of P, R, and $\varepsilon(T)$ in the population model of Eq. **1** gives the full temperature-dependent model of growth.

The Importance of Temperature-Dependent Allocation in an Experimental System

Next, we fitted the model for population growth to data from a laboratory experiment on *C. vulgaris* (2). In the experiments, net photosynthesis, respiration, and growth rate TPCs were measured for acclimated (10 generations) and adapted (100 generations) populations (*Materials and Methods*). The temperature-dependent $\varepsilon(T)$ was supported over a temperature-independent $\varepsilon(\kappa)$ (*SI Appendix*, Table S1). The inferred $\varepsilon(T)$ monotonically increased in both populations (Fig. 2*C*). We found that $\varepsilon(T)$ has a greater activation energy in adapted (0.64 eV $\pm$0.35 95% confidence interval) than in acclimated (0.53 eV $\pm$0.33) populations. Even though the confidence intervals of both E_ε and ε_0 overlap (Eq. **4** and *SI Appendix*, Table S2), Fig. 2*C* shows that adapted populations allocated a greater proportion of the carbon flux to growth and that this proportion increased more rapidly with temperature than that for acclimated populations. Finally, both ΔE_r and $\Delta T_{\text{pk},r}$ (Eqs. **5** and **6**) were positive; i.e., both activation energies and $T_{\text{pk},r}$ increased due to the temperature dependence of allocation efficiency (Fig. 3). As expected from theory (*Theory* above and *SI Appendix*, section S5), $\Delta E_r = E_\varepsilon$ for both acclimated and adapted populations. The change in $T_{\text{pk},r}$ due to $\varepsilon(T)$ ($\Delta T_{\text{pk},r}$) was also positive, although the growth rate TPC for adapted populations did not peak within the experimental temperature range.

In addition to the model of Eq. **1**, we also fitted an alternative, structurally different, but biologically feasible model (*SI Appendix*, section S9). In contrast to Eq. **1**, in this alternative model, $\varepsilon(T)$ limits how much fixed carbon is available to the cell before respiration occurs. The results show that Eq. **1** is better supported for both acclimated and adapted populations (*SI Appendix*, Table S1).

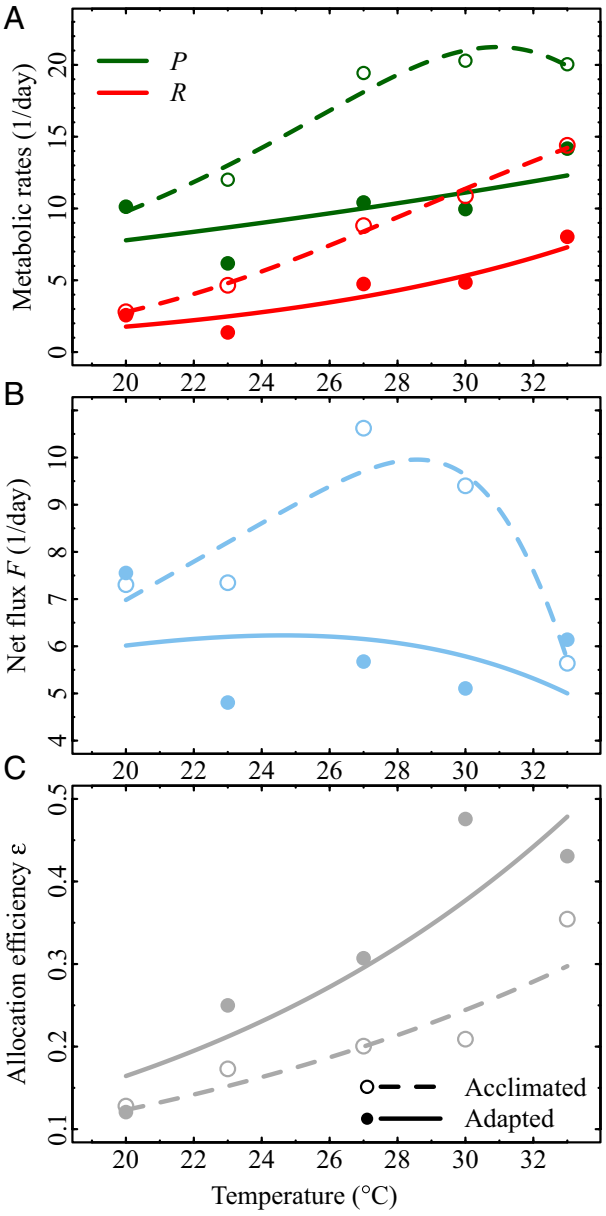

Fig. 2. Metabolic rates and allocation efficiencies for experiments on acclimated and adapted *C. vulgaris* populations. (*A*) Net photosynthesis *P* and dark respiration rates *R*. (*B*) Net flux *F*. (*C*) BA $\varepsilon(T)$ (with E_ε of 0.53 eV and 0.64 eV for acclimated and adapted populations, respectively; *SI Appendix*, Table S2). Dashed lines and open circles are for acclimated responses (10 generations) and solid lines and solid circles are for adapted responses (100 generations). Circles correspond to the means of three replicate experimental values at each growth temperature.

The Effect of ε on Potential Growth Rates Across Species

Finally, we explore how $\varepsilon(T)$ might affect the shape of the growth rate TPC across a wide diversity of species. We calculated the potential growth rate TPCs (Eq. **1**) for 38 aquatic and terrestrial autotroph species for which coupled P and R TPCs were available, assuming different levels of temperature dependence of $\varepsilon(T)$ (e.g., Fig. 1 and *Materials and Methods*). We parameterized $\varepsilon(T)$ by choosing a value of ε_0 (Eq. **4**) that

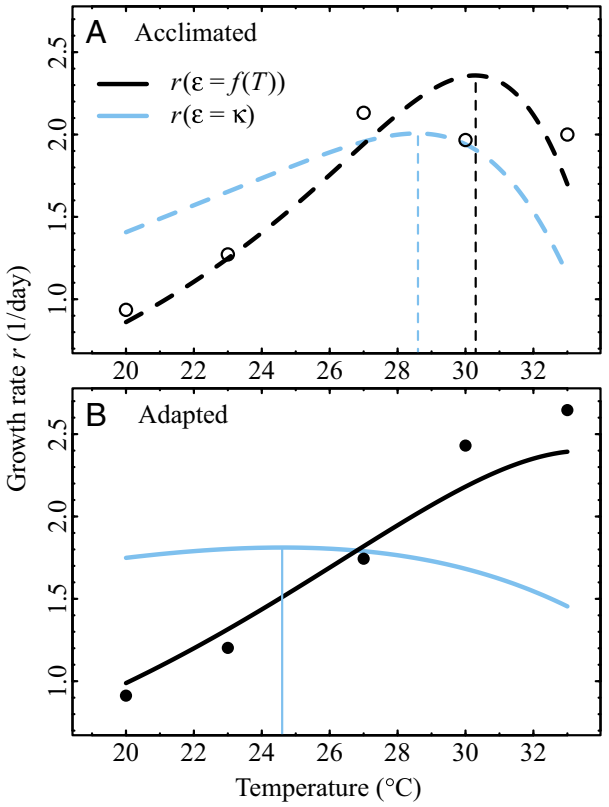

Fig. 3. Growth rates with temperature-independent and -dependent ε, for experiments on acclimated and adapted *C. vulgaris* populations. (*A* and *B*) Growth rates for (*A*) acclimated and (*B*) adapted populations. Light blue lines are for growth assuming a temperature-independent $\varepsilon(\kappa)$, while black lines are for growth with the $\varepsilon(T)$ of Fig. 2*C*. Vertical lines correspond to the respective $T_{\mathrm{pk},r}$ values. ΔE_r (Eq. **5**) was 0.53 eV and 0.64 eV for acclimated and adapted populations, respectively, corresponding to the values of E_ε (Fig. 2*C*) and thus in line with theoretical expectations. $\Delta T_{\mathrm{pk},r}$ (Eq. **6**) was 1.7 °C and over 8.4 °C for acclimated and adapted populations, respectively. Circles correspond to the means of three replicate experimental values at each growth temperature.

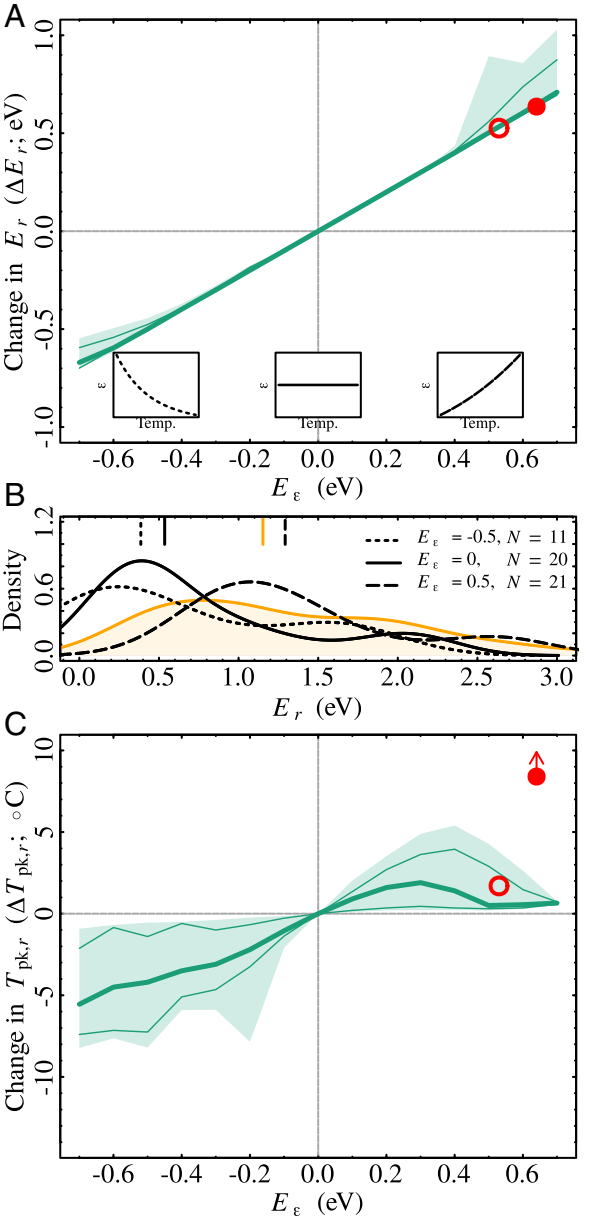

Fig. 4. Impact of temperature dependence in ε on E_r and $T_{\mathrm{pk},r}$. (*A*) ΔE_r (Eq. **5**) as a function of the activation energy of $\varepsilon(T)$ for the 21 aquatic populations. (*B*) Theoretical distributions of E_r for different E_ε values (black lines) juxtaposed against the empirically observed distribution for phytoplankton (orange line) (see *SI Appendix*, Fig. S8 for analogous results for combined terrestrial and aquatic species). The vertical lines mark the median activation energies for the respective distributions; note that median activation energy when $E_\varepsilon > 0$ is closest to that of the empirical distribution. (*C*) $\Delta T_{\mathrm{pk},r}$ as a function of the activation energy of $\varepsilon(T)$. For example, $\Delta E_r = 0.2$ in *A* means that when E_r is estimated with $\varepsilon(T)$, it is 0.2 eV higher than when E_r is calculated with $\varepsilon(\kappa)$ (Eq. **5**). Similarly, $\Delta T_{\mathrm{pk},r} = -5$ in *C* means that potential growth estimated with a temperature-dependent $\varepsilon(T)$ peaks at a temperature 5 °C lower than when growth is calculated with $\varepsilon(\kappa)$ (Eq. **6**). The shaded areas in *A* and *C* range from 12.5th to 87.5th percentiles across all potential growth rates, thin lines are the 25th and 75th percentiles, and the thick lines are the 50th percentiles. For a specific example with a single pair of *P* and *R* curves, see Fig. 1 *D* and *E*. Red circles in *A* and *C* show ΔE_r and $\Delta T_{\mathrm{pk},r}$ observed in the laboratory experiments on *C. vulgaris*: Open and solid circles are for acclimated and adapted populations, respectively (Fig. 3). The growth TPC for the adapted population did not peak within the experimental range, so the arrow on the solid red circle in *C* indicates that the value is a minimum bound on $\Delta T_{\mathrm{pk},r}$.

ensured that between the minimum experimental temperature and $T_{\mathrm{pk},P}$, half of the total available carbon was allocated to growth (*SI Appendix*, section S6). Then, we estimated the impact of temperature dependence of $\varepsilon(T)$ (E_ε) on both the activation energy (E_r) and the optimal temperature ($T_{\mathrm{pk},r}$) of potential growth. We also compared the resulting distributions of activation energies of potential growth rate TPCs with an empirical distribution estimated from growth TPCs measured in laboratory experiments (*Materials and Methods*). Because only phytoplankton growth rate data were available for this comparison, here we focus on the potential growth rates calculated for aquatic species only (results including terrestrial species are in *SI Appendix*, section S12.1).

Our results show that $\varepsilon(T)$ can substantially alter the activation energy of growth rate (E_r) across species (Fig. 4*A*). The change in E_r (ΔE_r) due to $\varepsilon(T)$ is directly proportional to E_ε, as predicted by the theory (*SI Appendix*, section S5). That is, when $\varepsilon(T)$ increases with T ($E_\varepsilon > 0$, as found in the laboratory experiments), potential growth curves become more sensitive to temperature. Conversely, when $\varepsilon(T)$ decreases with temperature ($E_\varepsilon < 0$), potential growth TPCs become less temperature sensitive. Overall, as seen in Fig. 4*B*, the distribution of activation energies of potential growth rates depends on the temperature sensitivity of $\varepsilon(T)$; the distribution becomes more right skewed as E_ε declines (from positive to negative values). Comparing

the theoretical activation energy distributions to the empirical one (orange line in Fig. 4*B*) suggests that a positive temperature dependence of E_ε is the most likely scenario in autotrophs (see *SI Appendix*, section S12.5 for a more detailed discussion), as was also observed in the experimental data (Fig. 2*C*).

The optimal temperature for potential growth rates, $T_{\mathrm{pk},r}$, also varied systematically with the temperature dependence of $\varepsilon(T)$ (Fig. 4*C*). The response was qualitatively consistent across species: Negative (respectively positive) activation energies of $\varepsilon(T)$ lowered (respectively increased) $T_{\mathrm{pk},r}$ relative to $\varepsilon(\kappa)$. However, the degree to which $T_{\mathrm{pk},r}$ changed varied across taxa, as evidenced by the wide shaded areas in Fig. 4*C*, meaning that the magnitude of $\Delta T_{\mathrm{pk},r}$ depends on the specific shape of the species' underlying metabolic rate TPCs. The effect of $\varepsilon(T)$ on $T_{\mathrm{pk},r}$ can be substantial: For $E_\varepsilon = -0.6$ eV, the median $\Delta T_{\mathrm{pk},r}$ is $-4.5\,^\circ$C. The effect is also asymmetrical and nonlinear: For $E_\varepsilon = 0.6$ eV, median $\Delta T_{\mathrm{pk},r}$ is $0.6\,^\circ$C. Note, however, that for the larger values of $|E_\varepsilon|$, many potential growth curves do not peak at all within the experimental temperature range. These were excluded from Fig. 4*C* and thus likely bias the asymmetry of the pattern. For example, the growth rate TPC for adapted populations of *C. vulgaris* did not peak within the experimental temperature range (Fig. 3*B*), perhaps explaining why the corresponding solid red circle in Fig. 4*C* falls outside the shaded area.

While Fig. 4 shows results for aquatic species only, patterns remain qualitatively similar when also including terrestrial species (*SI Appendix*, Fig. S8). These results are also largely robust to how $\varepsilon(T)$ is parameterized (*SI Appendix*, section S12); with an alternative parameterization of Eq. **4**, the relationship between ΔE_r and E_ε remains the same (*SI Appendix*, Fig. S9*A*), while the pattern between $\Delta T_{\mathrm{pk},r}$ and E_ε changes quantitatively, but not qualitatively (*SI Appendix*, Fig. S9*C*).

Discussion

We have presented a mathematical model for the temperature dependence of exponential growth rates in populations of photosynthetic autotroph cells and used data to both test the theory and understand how the temperature dependence of carbon allocation efficiency contributes to shape growth rate TPCs across a diversity of species. Our results show that temperature dependence in carbon allocation efficiency can be a significant factor in determining the shape of the TPCs of growth rates.

The laboratory experiments on a phytoplankton species (the single-celled green alga *C. vulgaris*) show that in this species, allocation efficiency ε is temperature dependent, with exponentially increasing allocation of intracellular carbon to growth with warming. This temperature dependence of $\varepsilon(T)$ in *C. vulgaris* leads to both a higher activation energy E_r and optimal temperature $T_{\mathrm{pk},r}$ of the growth rate TPC, compared with if ε had been assumed to be temperature independent. Padfield et al. (2) previously hypothesized that carbon use efficiency (CUE), a measure of growth "potential" defined as the ratio of net and gross photosynthesis (*SI Appendix*, section S1.4), plays an important role in the evolution of elevated thermal tolerance in phytoplankton. Here we have shown that it is in fact the marked increase in efficiency of carbon allocation to growth that allowed this evolution of tolerance to high temperature. This increase in carbon allocation efficiency with evolution may result from diversion of metabolic energy away from maintenance and repair [reflected in the high respiration rates of the nonevolved populations at high temperature (Fig. 2)], and toward growth.

Our further investigation of the effect of $\varepsilon(T)$ on potential growth rates across a diverse group of aquatic species showed that despite considerable variation in paired photosynthesis and respiration TPCs, the impact of a temperature-dependent $\varepsilon(T)$ was very consistent across these species. Comparing distributions of activation energies of predicted growth rates with real data suggests that allocation efficiency is likely to increase with temperature across most aquatic autotroph species. This result implies that activation energies of growth rate are expected to be higher than activation energies for net flux. We note that although this analysis focused on aquatic species, the model should also apply to tissue growth in terrestrial plants using locally fixed carbon (e.g., leaves in shoots of young saplings). However, we were unable to find sufficient data on growth rates of such tissues across sufficient multiple temperatures with which to create an empirical distribution of activation energies and perform an analogous comparison for terrestrial plants.

The effect of allocation efficiency $\varepsilon(T)$ on the potential growth rate TPC depends on its temperature dependence in the operational temperature range (the increasing part of the growth TPC, expected to be the ecologically most relevant temperature range). If $\varepsilon(T)$ increases (respectively decreases) with temperature, its effect is likely to increase (respectively decrease) both the activation energy of the potential growth rate TPC (E_r) and the optimal temperature for potential growth ($T_{\mathrm{pk},r}$). This result qualitatively holds irrespective of the specific shape of $\varepsilon(T)$ (*SI Appendix*, section S12). The effect of $\varepsilon(T)$ on the activation energy of potential growth rates is very predictable, while the impact on $T_{\mathrm{pk},r}$, while qualitatively consistent, is more variable across species and less quantitatively predictable. The reason is simple: When $\varepsilon(T)$ increases with temperature, $T_{\mathrm{pk},r}$ can only be greater than $T_{\mathrm{pk},F}$, but the difference between the two is contingent on the specific shape of the underlying metabolic rate TPCs. When net flux around its peak is relatively insensitive to temperature, it takes only moderate temperature dependence in $\varepsilon(T)$ to substantially change $T_{\mathrm{pk},r}$, while when net flux is strongly temperature dependent around its peak, a greater temperature dependence in $\varepsilon(T)$ is necessary to change $T_{\mathrm{pk},r}$.

The model can also be extended to explore how uptake of a limiting nutrient (other than carbon, which is typically not limiting in natural environments) may interact with allocation efficiency to affect the shape of potential growth rate TPCs. For instance, let

$$r = V_{\mathrm{n}}\,\varepsilon\,F, \qquad [7]$$

where V_{n} is a dimensionless Michaelis–Menten nutrient uptake term which can be theoretically approximated as a monotonically decreasing function of temperature (*SI Appendix*, section S1.3) (10, 42). In this case, nutrient limitation lowers both E_r and $T_{\mathrm{pk},r}$ (*SI Appendix*, Fig. S13). Similar results were obtained by Thomas et al. (43) with a temperature-independent nutrient uptake, although their model was closer to our alternative model structure (*SI Appendix*, sections S1.5 and S9), where nutrient limitation affects carbon fixation only in photosynthesis. Nutrient limitation could then interact with $\varepsilon(T)$ and, where $\varepsilon(T)$ increases with temperature, counteract its effects on the potential growth rate TPC [by offsetting the increases in both E_r and $T_{\mathrm{pk},r}$ due to $\varepsilon(T)$] or, where $\varepsilon(T)$ decreases with temperature, compound its effects by further reducing E_r and $T_{\mathrm{pk},r}$ (*SI Appendix*, Fig. S14). Thus, nutrient limitation would be expected to reduce both the sensitivity of potential growth rates to increases in temperature and the optimal temperature for growth. Despite these predictions from our model, further experiments would be necessary to elucidate whether nutrient availability nonlinearly affects allocation efficiency and its temperature dependence; nutrient limitation could conceivably systematically alter how carbon is allocated.

Our model is intended to apply to unicellular autotrophs (phytoplankton) and other cell populations that use carbon fixed by those cells such as in elongating leaves of terrestrial plants and aquatic macrophytes and shoots of all young multicellular plants (e.g., small saplings). In terrestrial "higher" plants, leaves constitute a single component of a more complex system,

and, as a result, $\varepsilon(T)$ could additionally encapsulate carbon that is reallocated to nonphotosynthetic tissue. The findings of our meta-analysis hold even when terrestrial and aquatic species are analyzed together (*SI Appendix*, section S12.4). However, the model could be expanded to include growth of the whole plant (including nonphotosynthetic tissue). At its simplest, an additional respiration term would be necessary in Eq. **1**, to account for nonphotosynthetic tissues. Preferably, nonphotosynthetic biomass could be tracked in an additional, coupled differential equation that would allow for carbon to be transferred between the two components. Such a model would require additional data that are not easily measurable. Understanding how adaptation might be expected to affect TPCs, as a function of long-term changes in temperature and time, also requires further work. The model, currently formulated in rates per day, could be elaborated to explicitly account for adaptation over longer timescales by, for example, letting the parameters that define P, R, and ε (e.g., activation energies and normalization constants) be functions of adaptation temperature and time (e.g., ref. 39). Here too, a more substantial volume of data, to include how TPCs vary over time, would be required.

Overall, these findings challenge the common assumption that allocation efficiency is temperature independent (10, 20, 24, 39) and suggest that to understand the link between intraspecific growth rate TPCs and underlying metabolic rates, it is important to include the temperature dependence of the allocation efficiency. In the metabolic theory of ecology (25, 26, 44), growth rate TPCs are often used as a means to infer the temperature dependence of the underlying metabolism or vice versa (39). However, as shown by our meta-analysis, some of the observed variation in the growth rate TPCs (38) may stem from variation in the temperature dependence of allocation efficiency and not be due to that in metabolic rates. Thus, studies that use growth rate TPCs as proxies for the TPCs of metabolism but ignore $\varepsilon(T)$ may reach biased conclusions. More generally, allocation efficiency in heterotrophs (commonly referred to as mass-conversion efficiency in the literature; e.g., ref. 45) has already been shown to broadly increase with temperature (46), and its consequences there also need to be explored more carefully.

Our work also shows that to make further progress toward understanding the temperature dependence of autotroph population growth rates, experimental data where growth rates, P, and R are measured in the same study are needed. Paucity of data is particularly acute in terrestrial species, where growth rates (in terms of mass) of leaves and shoots are seldom collected across multiple temperatures. Even when all three rates are measured in the same study, usually in aquatic species (e.g., ref. 3), establishing the mechanistic link between a growth rate on the one hand and the underlying metabolic rates on the other hand would require that both are measured at comparable timescales. For example, in phytoplankton, metabolic rates are often measured as acute responses to a change in temperature in short experiments (the order of minutes), while growth rates may take days to estimate. This difference might potentially introduce a confounding effect of acclimation in the processes underlying allocation of carbon to growth [i.e., $\varepsilon(T)$]. With appropriate data, $\varepsilon(T)$ can then be estimated by fitting our model directly (as done here) or, alternatively, by fitting different formulations of $\varepsilon(T)$ to $r/F = r/(P-R)$.

Finally, further work is required to unpack the metabolic processes involved in allocation efficiency and thus provide a more mechanistic link between population growth and individual metabolism. For example, the role played by respiration is greatly simplified in this model: It simply reduces how much carbon is available to the cells. However, growth can be constrained by respiration (47, 48); its products, such as energy and carbon skeletons, are essential for growth, maintenance, and transport processes (12, 15, 49, 50). However, the efficiency with which these products are generated can depend on which one is in greatest demand (48), which in turn may affect our estimated allocation efficiency. Under certain conditions, alternative (less "efficient") respiratory pathways may also be activated (47, 51), which would further complicate the link between the measured use of carbon through respiration and growth. To what extent these respiratory processes are reflected in P and R is unclear, and some elements may in fact be captured in ε (13). We also exclusively focus on the effect of temperature on allocation efficiency. However, other (potentially covarying) environmental variables could interact with temperature to affect ε. For instance, external CO_2 concentration affects metabolic rates (22, 23, 52), and under water stress growth in terrestrial plants is reduced (23) as cells accumulate carbon to maintain osmotic balance. These and other factors such as light availability may well result in systematic differences in the temperature dependence of ε between terrestrial and aquatic autotrophs, which we are currently unable to detect in the available experimental data.

In conclusion, our model and empirical results link, in the simplest possible way, the temperature dependence of the underlying metabolic rates and allocation, with exponential population or somatic growth in autotrophs. While more detailed models of exponential growth rates have been previously published (28, 31, 32, 53, 54), none of these explicitly consider the temperature dependence of underlying metabolic rates. Our results provide a framework for experimentalists that requires data for only three frequently measured rates (growth rate, net photosynthesis, and dark respiration) across temperatures, to determine the TPC of allocation efficiency $\varepsilon(T)$, a prerequisite for developing more complex, mechanistic models. The simplicity of our approach means that it has the potential to be used and applied to explore and uncover broader patterns in the metabolic basis for the temperature dependence of growth rates in autotrophs.

Materials and Methods

Experimental Data on *C. vulgaris*. Full details on the experimental setup can be found in ref. 2 and more information is provided in *SI Appendix*, section S10; we here provide a summary. Three replicate populations of *C. vulgaris* were established per five different growth temperatures (20 °C, 23 °C, 27 °C, 30 °C, and 33 °C). Exponential growth rates were estimated for each growth temperature after ∼10 ("acclimated") and 100 ("adapted") generations. Padfield et al. (2) also measured the acute short-term responses of metabolic rates (net photosynthesis *P* and dark respiration *R*) to a range of temperatures for each of the populations grown at the five growth temperatures, after both 10 and 100 generations. Data used from these experiments are available online (55).

Acute responses of metabolic rates to a change in temperature are typically measured in brief (order of minutes) experiments in stressful conditions for the cells. On the other hand, growth rate experiments take longer (order of days), to ensure maximum exponential growth rates are captured. To allow the most direct comparison between metabolic rates and growth rates, we needed acclimated and adapted responses of metabolic rates. We fitted the Schoolfield–Sharpe model (Eq. **3**) to each acute response and used the model to estimate the metabolic rates at the culture's corresponding growth temperature (i.e., we estimated *P* and *R* at 20 °C for the cultures acclimated and adapted to 20 °C, at 23 °C for the cultures grown at 23 °C, and so on; *SI Appendix*, Fig. S6). When fitting the models to the data, we averaged metabolic rates and growth rates across the three replicates. As a result, we had experimental values of *P*, *R*, and growth rates, for both acclimated and adapted responses. For the alternative model structure (*SI Appendix*, section S9), we assumed that gross photosynthesis $P_g \approx P + R_l$ (where R_l is daytime respiration) and that $R \approx R_l$ (2).

Potential Growth Rate TPCs Across a Range of Autotroph Species. We compiled a database of intraspecific TPCs of net photosynthesis and respiration extracted from the literature. We digitized data from tables, text, or figures, using DataThief (56) and Plot Digitizer (57), and, when possible, contacted authors to obtain raw data. Most TPCs were measured under saturated light conditions and ambient or saturating CO_2 concentrations (not all

studies reported this information). In all cases, metabolic rates were measured on photosynthetic tissue only; thus, in higher terrestrial plants, rates were measured on leaves only.

Metabolic rates are usually single peaked across their full thermal range; some studies, however, focused on a narrower temperature range such that TPCs can consist of a rise or fall in the trait only. We are specifically interested in the operational temperature range, which typically comprises the rise of a rate up to its maximum value. To be able to accurately characterize this rise in rates with temperature when fitting the Schoolfield–Sharpe model to the data, we kept curves with at least three data points below the rates' T_{pk} and at least five data points in total. We also removed curves with activation energies greater than three, as higher values are often due to poor fits of the model to the data or the result of performing the experiment over a narrow temperature range (17). Because we were interested in how P and R interact with $\varepsilon(T)$ to produce a potential intraspecific growth rate TPC, we kept curves for which both P and R were measured in the same experiment. For experiments in which multiple TPCs were available for the same species and rate, we kept the curve with the highest coefficient of determination R^2. Allocation efficiency $\varepsilon(T)$ can be expected to differ between species and taxonomic groups. However, to be able to parameterize $\varepsilon(T)$ in a way that could allow comparisons across species, we required a fixed reference point common to all curves (*SI Appendix*, section S6). Because species' operational temperature ranges are likely to be limited, on the upper range, by the temperature at which photosynthesis peaks (17, 58), we discarded pairs of curves for which net photosynthesis did not peak within the experimental temperature range. We also excluded pairs of curves for which net flux was negative for $T < T_{pk,P}$, because the model implicitly assumes positive net fluxes. The result was a database with 43 pairs of P and R TPCs (21 aquatic and 22 terrestrial species) for 38 different species, from 27 sources. The rates were integrated over 24 h (giving the total amount of O_2 or CO_2 per unit mass or area per day). Rates were measured in a variety of different units (μmol O_2 or CO_2 per unit kg dry weight, fresh weight, chlorophyll, cell, or area per unit time), making comparisons between pairs of curves difficult. We were specifically interested in the impacts of $\varepsilon(T)$ on the qualitative temperature dependence of the potential growth rate. For this reason, for each pair of curves, we normalized both P and R curves using the peak net photosynthetic rate (P_{pk}), i.e., P/P_{pk} and R/P_{pk}. Thus, the maximum net photosynthetic rate was equal to one for all species, while maintaining the relative shapes of the P and R curves. For this reason, the metabolic rates and resultant growth rates are unitless. Processed data (with unitless normalization constants and integration over 24 h) are provided in Dataset S2.

We describe $\varepsilon(T)$ as a BA function [Eq. **4** and Fig. 1*B*; although we also use a quadratic $\varepsilon(T)$ in *SI Appendix*, sections S6 and S12]. The degree of temperature dependence of $\varepsilon(T)$ (E_ε in Eq. **4**) was set and varied to assess its effect on the potential growth rate TPC. The maximum $|E_\varepsilon|$ was comparable to the value observed in the *C. vulgaris* laboratory experiments (Fig. 2*C*). We then introduced each $\varepsilon(T)$ TPC, together with each pair of P and R curves, into Eq. **1** to produce a potential growth rate TPC for each population and value of E_ε. The activation energy of potential growth rates E_r was estimated by fitting a Schoolfield–Sharpe model (Eq. **3**) to the growth rate TPC (with adjustments described in *SI Appendix*, section S7 to ensure acceptable fits; also see *SI Appendix*, section S8). When estimating the change in E_r due to $\varepsilon(T)$, potential growth rate TPCs which, due to $\varepsilon(T)$, declined only with temperature were excluded from this analysis. Similarly, when estimating the change in $T_{pk,r}$ due to $\varepsilon(T)$, potential growth rate TPCs that did not peak within the experimental temperature range were excluded.

To test the robustness of our results, we also used an alternative approach to parameterize $\varepsilon(T)$ (Eq. **4** and *SI Appendix*, section S6); results for this alternative parameterization are given in *SI Appendix*, section S12.

Real Growth Rate TPCs Across a Range of Phytoplankton Species. To compare distributions of activation energies for the potential growth rates of aquatic species against activation energies of real, measured growth rates, we compiled a database of phytoplankton growth rate TPCs (taken mainly from refs. 20 and 59–61). Growth rates were estimated under light- and nutrient-saturated conditions. We removed curves that had an activation energy greater than four, and for species with replicate activation energies we kept values corresponding to the fit with the highest R^2. The result was 165 estimates (each for an individual taxon) of activation energy for phytoplankton growth rate TPCs. Activation energies are provided in Dataset S1.

Statistical Methods. Fitting in all cases was performed using the "nlsLM" function in the "minpack.lm" package in R (62), which uses the Levenberg–Marquardt optimization algorithm for nonlinear least-squares fitting. To ensure the best fit was found, the algorithm was run with 1,000 randomized starting parameters, keeping the fit with the lowest corrected AIC (AICc) score (63). The Sharpe–Schoolfield model was fitted to TPCs of metabolic and growth rates on the ln scale, and all fits with $R^2 < 0.5$ were excluded.

Model comparisons (between different combinations of model structures and temperature dependences of $\varepsilon(T)$; *SI Appendix*, section S11) were performed on the basis of AIC scores. The population model was fitted on the linear scale.

ACKNOWLEDGMENTS. We thank Mridul Thomas and Van Savage for valuable discussions and comments on previous versions of the manuscript. We also thank three anonymous reviewers for comments and suggestions that helped substantially improve the manuscript. This study was supported by Natural Environment Research Council Grant NE/M003205/1 (to S.P. and G.Y.-D.), and a Science and Solutions for a Changing Planet Doctoral Training Partnership scholarship (to D.-G.K.).

1. Way DA, Oren R (2010) Differential responses to changes in growth temperature between trees from different functional groups and biomes: A review and synthesis of data. *Tree Physiol* 30:669–688.
2. Padfield D, Yvon-Durocher G, Buckling A, Jennings S, Yvon-Durocher G (2016) Rapid evolution of metabolic traits explains thermal adaptation in phytoplankton. *Ecol Lett* 19:133–142.
3. Schaum CE, et al. (2017) Adaptation of phytoplankton to a decade of experimental warming linked to increased photosynthesis. *Nat Ecol E* 1:0094.
4. Angilletta MJ, Steury TD, Sears MW (2004) Temperature, growth rate, and body size in ectotherms: Fitting pieces of a life-history puzzle. *Integr Comp Biol* 44:498–509.
5. Knies JL, Kingsolver JG, Burch CL (2009) Hotter is better and broader: Thermal sensitivity of fitness in a population of bacteriophages. *Am Nat* 173:419–430.
6. Houghton RA, et al. (2000) Annual fluxes of carbon from deforestation and regrowth in the Brazilian Amazon. *Nature* 403:301–304.
7. Clark DA, Piper SC, Keeling CD, Clark DB (2003) Tropical rain forest tree growth and atmospheric carbon dynamics linked to interannual temperature variation during 1984–2000. *Proc Natl Acad Sci USA* 100:5852–5857.
8. García-Carreras B, Reuman DC (2013) Are changes in the mean or variability of climate signals more important for long-term stochastic growth rate? *PLoS One* 8:e63974.
9. IPCC, Core Writing Team (2014) Climate change 2014: Synthesis report. *Contribution of Working Groups I, II and III to the Fifth Assessment Report of the Intergovernmental Panel on Climate Change,* eds Pachauri RK, Meyer LA (IPCC, Geneva), pp 35–112.
10. Reuman DC, Holt RD, Yvon-Durocher G (2014) A metabolic perspective on competition and body size reductions with warming. *J Anim Ecol* 83:59–69.
11. Gandhi SR, Yurtsev EA, Korolev KS, Gore J (2016) Range expansions transition from pulled to pushed waves as growth becomes more cooperative in an experimental microbial population. *Proc Natl Acad Sci USA* 113:6922–6927.
12. Raven JA (1976) The quantitative role of 'dark' respiratory processes in heterotrophic and photolithotropic plant growth. *Ann Bot* 40:587–602.
13. Amthor JS (1984) The role of maintenance respiration in plant growth. *Plant Cell Environ* 7:561–569.
14. Del Giorgio PA, Cole JJ (1998) Bacterial growth efficiency in natural aquatic systems. *Annu Rev Ecol Syst* 29:503–541.
15. Amthor JS, Baldocchi DD (2001) *Terrestrial Global Productivity: Past, Present and Future*, eds Roy J, Mooney HA, Saugier B (Academic, San Diego), pp 33–52.
16. Schoolfield RM, Sharpe PJH, Magnuson CE (1981) Non-linear regression of biological temperature-dependent rate models based on absolute reaction-rate theory. *J Theor Biol* 88:719–731.
17. Pawar S, Dell AI, Savage VM, Knies JI (2016) Real versus artificial variation in the thermal sensitivity of biological traits. *Am Nat* 187:E41–E52.
18. Farquhar GD, von Caemmerer S, Berry JA (1980) A biochemical model of photosynthetic CO_2 assimilation in leaves of C_3 species. *Planta* 149:78–90.
19. Raven JA, Geider RJ (1988) Temperature and algal growth. *New Phytol* 110:441–461.
20. López-Urrutia Á, San Martin E, Harris RP, Irigoien X (2006) The metabolic balance of the oceans. *Proc Natl Acad Sci USA* 103:8739–8744.
21. Allen AP, Gillooly JF, Brown JH (2005) Linking the global carbon cycle to individual metabolism. *Funct Ecol* 19:202–213.
22. de Kluijver A, et al. (2010) Phytoplankton-bacteria coupling under elevated CO_2 levels: A stable isotope labelling study. *Biogeosciences* 7:3783–3797.
23. Ryan MG (1991) Effects of climate change on plant respiration. *Ecol App* 1:157–167.
24. Baird ME, Emsley SM, McGlade JM (2001) Modelling the interacting effects of nutrient uptake, light capture and temperature on phytoplankton growth. *J Plankton Res* 23:829–840.
25. Brown JH, Gillooly JF, Allen AP, Savage VM, West GB (2004) Toward a metabolic theory of ecology. *Ecology* 85:1771–1789.
26. Savage VM, Gillooly JF, Brown JH, West GB, Charnov EL (2004) Effects of body size and temperature on population growth. *Am Nat* 163:429–441.
27. Huey RB, Kingsolver JG (2011) Variation in universal temperature dependence of biological rates. *Proc Natl Acad Sci USA* 108:10377–10378.
28. Droop MR (1973) Some thoughts on nutrient limitation in algae. *J Phycol* 9:264–272.

29. Kooijman SALM (2000) *Dynamic Energy and Mass Budgets in Biological Systems* (Cambridge Univ Press, Cambridge, UK).
30. Bonachela JA, Michael R, Levin SA (2011) Dynamic model of flexible phytoplankton nutrient uptake. *Proc Natl Acad Sci USA* 108:20633–20638.
31. Kempes CP, Dutkiewicz S, Follows MJ (2012) Growth, metabolic partitioning, and the size of microorganisms. *Proc Natl Acad Sci USA* 109:495–500.
32. Weiße AY, Oyarzún DA, Danos V, Swain PS (2015) Mechanistic links between cellular trade-offs, gene expression, and growth. *Proc Natl Acad Sci USA* 112:E1038–E1047.
33. Kempes CP, Wang L, Amend JP, Doyle J, Hoehler T (2016) Evolutionary tradeoffs in cellular composition across diverse bacteria. *ISME J* 10:2145–2157.
34. Baines SB, Pace ML (1991) The production of dissolved organic matter by phytoplankton and its importance to bacteria: Patterns across marine and freshwater species. *Limnol Oceanogr* 36:1078–1090.
35. Engel A, Thoms S, Riebesell U, Rochelle-Newall E, Zondervan I (2004) Polysaccharide aggregation as a potential sink of marine dissolved organic carbon. *Nature* 428:929–932.
36. Falkowski PG, Barber RT, Smetacek V (1998) Biogeochemical controls and feedbacks on ocean primary production. *Science* 281:200–206.
37. Kontopoulos DG, García-Carreras B, Sal S, Smith TP, Pawar S (2018) Use and misuse of temperature normalisation in meta-analyses of thermal responses of biological traits. *PeerJ* 6:e4363.
38. Dell AI, Pawar S, Savage VM (2011) Systematic variation in the temperature dependence of physiological and ecological traits. *Proc Natl Acad Sci USA* 108:10591–10596.
39. Luhring T, DeLong JP (2017) Scaling from metabolism to population growth rate to understand how acclimation temperature alters thermal performance. *Integr Comp Biol* 57:103–111.
40. Follows MJ, Dutkiewicz S, Grant S, Chisholm SW (2007) Emergent biogeography of microbial communities in a model ocean. *Science* 315:1843–1846.
41. Dell AI, Pawar S, Savage VM (2014) Temperature dependence of trophic interactions are driven by asymmetry of species responses and foraging strategy. *J Anim Ecol* 83:70–84.
42. Aksnes DL, Egge JK (1991) A theoretical model for nutrient uptake in phytoplankton. *Mar Ecol Prog Ser* 70:65–72.
43. Thomas MK, et al. (2017) Temperature-nutrient interactions exacerbate sensitivity to warming in phytoplankton. *Glob Change Biol* 23:3269–3280.
44. Gillooly JF, Brown JH, West GB, Savage VM, Charnov EL (2001) Effects of size and temperature on metabolic rate. *Science* 293:2248–2251.
45. Vucic-Pestic O, Ehnes RB, Rall BC, Brose U (2011) Warming up the system: Higher predator feeding rates but lower energetic efficiencies. *Glob Change Biol* 17:1301–1310.
46. Lang B, Ehnes RB, Ulrich B, Rall BC (2017) Temperature and consumer type dependencies of energy flows in natural communities. *Oikos* 126:1717–1725.
47. Amthor JS (1994) *Physiology and Determination of Crop Yield*, eds Boote KJ, Bennett JM, Sinclair TR, Paulsen GM (Am Soc Agron, Madison, WI), pp 221–250.
48. Amthor JS (1994) *Ecophysiology of Photosynthesis*, eds Schulze ED, Caldwell MM (Springer, Berlin), pp 71–101.
49. Atkin OK, Bruhn D, Hurry VM, Tjoelker MG (2005) The hot and the cold: Unravelling the variable response of plant respiration to temperature. *Func Plant Biol* 32: 87–105.
50. Allison SD (2014) Modeling adaptation of carbon use efficiency in microbial communities. *Front Microbiol* 5:571.
51. Amthor JS (1995) Terrestrial higher-plant response to increasing atmospheric [CO_2] in relation to the global carbon cycle. *Glob Change Biol* 1:243–274.
52. Riebesell U (2004) Effects of CO_2 enrichment on marine phytoplankton. *J Oceanogr* 60:719–729.
53. Shutter B (1979) A model of physiological adaptation in unicellular algae. *J Theor Biol* 78:519–552.
54. Geider RJ, MacIntyre HL, Kana TM (1997) Dynamic model of phytoplankton growth and acclimation: Responses of the balanced growth rate and the chlorophyll a-carbon ratio to light, nutrient-limitation and temperature. *Mar Ecol Prog Ser* 148:187–200.
55. Padfield D (2018) Data from "Padfield et al. (2016) Rapid evolution of metabolic traits explains thermal adaptation in phytoplankton. Ecology letters." Zenodo. doi.org/10.5281/zenodo.1285673 (Version v1.0).
56. Tummers B (2006) Datathief III. Available at https://datathief.org/. Accessed March 1, 2015.
57. Huwaldt JA (2015) Plot digitizer. Available at plotdigitizer.sourceforge.net/. Accessed March 1, 2015.
58. Martin TL, Huey RB (2008) Why "suboptimal" is optimal: Jensen's inequality and ectotherm thermal performance. *Am Nat* 171:E102–E118.
59. Rose JM, Caron DA (2007) Does low temperature constrain the growth rates of heterotrophic protists? Evidence and implications for algal blooms in cold waters. *Limnol Oceanogr* 52:886–895.
60. Bissinger JE, Montagnes DJ, Atkinson D (2008) Predicting marine phytoplankton maximum growth rates from temperature: Improving on the Eppley curve using quantile regression. *Limnol Oceanogr* 53:487–493.
61. Thomas MK, Kremer CT, Klausmeier CA, Litchman E (2012) A global pattern of thermal adaptation in marine phytoplankton. *Science* 338:1085–1088.
62. Elzhov TV, Mullen KM, Spiess AN, Bolker B (2015) *minpack.lm: R Interface to the Levenberg-Marquardt Nonlinear Least Squares Algorithm Found in MINPACK, Plus Support for Bounds*. R package Version 1.2-0. Available at https://cran.r-project.org/web/packages/minpack.lm/index.html. Accessed March 1, 2015.
63. Hurvich CM, Tsai CL (1989) Regression and time series model selection in small samples. *Biometrika* 76:297–307.

Supplementary Information for
The role of carbon allocation efficiency in the temperature dependence of growth rates in autotrophs

Bernardo García-Carreras, Sofía Sal, Daniel Padfield,
Dimitrios - Georgios Kontopoulos, Elvire Bestion, C.-Elisa Schaum,
Gabriel Yvon-Durocher & Samrāt Pawar

Contents

Introduction

In this Supplementary Information, we provide more complete explanations and additional results. We include a fuller description of the population model in Section S1; the model presented in the main text is a subset of the material presented here. In Section S2 we provide a more mechanistic derivation of the temperature dependence of nutrient uptake, specific to aquatic autotrophs. We show how the shape of the net flux thermal performance curve (TPC; thus, excluding temperature dependence of ε) can change as a function of the differences in the underlying metabolic rates (P and R) in Section S3. Section S4 explains why we use the activation energy and optimal temperature as descriptors of the growth rate TPC. In Section S5, we derive the theoretically expected impact of an Boltzmann-Arrhenius $\varepsilon(T)$ on the activation energy of growth. In Sections S6 to S8, we describe different aspects of the methods used: Section S6 makes explicit what parameterisations we used for $\varepsilon(T)$ to generate Figs. 1 and 4 in the main text; Section S7 provides additional details on how we treated the simulated potential growth data to better fit the response functions; and Section S8 explains how small biases may be introduced in the estimates of the activation energy of growth rates, due to the sometimes small temperature range over which the activation energy is estimated. The population model is described in full using a specific model structure - however, alternative model structures are possible. These are given in Section S9, and we use the laboratory experiments on *Chlorella vulgaris* to infer the most likely model structure. We provide full details on the experiments used in the main text in Section S10, and details of the model fits to these experimental data in Section S11. In Section S12, we provide additional results. We show the results of the meta-analysis combining both aquatic and terrestrial species. In the main text we focus on the Boltzmann-Arrhenius $\varepsilon(T)$; we also test the robustness of our results by using an alternative parameterisation, as well as results using quadratic formulations of $\varepsilon(T)$. Finally, we demonstrate how $\varepsilon(T)$ would be expected to interact with the effects of nutrient limitation.

S1 The population model

We begin with the following model for the temperature (T) dependent biomass density N (µgC/m^3) of a population of photosynthetic autotroph cells in the exponential phase of growth:

$$\frac{1}{N}\frac{\mathrm{d}N}{\mathrm{d}t} = r = V_\mathrm{n}\,\varepsilon\,F, \tag{S1}$$

where F is net carbon flux (1/day), ε (dimensionless) is the allocation efficiency and captures the allocation of the available intracellular carbon to growth, and V_n (dimensionless) accounts for the effects of a limiting nutrient (other than carbon, which is typically not limiting in natural environments). Net carbon flux F (henceforth "net flux") is a measure of mass-specific growth potential, given by

$$F = P - R, \tag{S2}$$

$$= P_\mathrm{g} - R_\mathrm{l} - R \tag{S3}$$

where P is net photosynthesis (difference between maximum gross photosynthetic rate P_g in nutrient-saturated and optimal-light conditions and daytime respiration R_l), and R is night-time (dark) respiration. Thus, F (e.g., blue line in Fig. 1a in the main text) represents an upper bound for how much of the carbon fixed in photosynthesis is potentially

available to the cells for growth, after accounting for respiratory losses. V_{n} is the Michaelis-Menten kinetics model for nutrient uptake

$$V_{\mathrm{n}} = \frac{S}{K_S + S}, \tag{S4}$$

where S is the concentration of a single limiting nutrient (in µmol or gr of nutrients/m^3), and K_S is the half saturation parameter - the nutrient concentration at which $V_{\mathrm{n}} = 0.5$. All rates are integrated over a 24 hour period. The model we present in the main text assumes saturating nutrient concentrations, where, because $S \to \infty$ and $V_{\mathrm{n}} \approx 1$, the model simplifies to

$$r = \varepsilon F. \tag{S5}$$

This model structure mirrors that of autotroph models expressed in terms of a maximum growth rate $r_{\max}$ rather than the underlying metabolic rates (e.g., 1–3). Alternative model structures are also possible (see Section S9), where V_{n} and ε affect different model parameters, thereby altering their interpretation. The model assumes that the main factor (other than the single nutrient captured by V_{n}) limiting growth is carbon availability. Where possible, we preferentially use Eq. (S2) because it uses rates typically measured in experiments. Note that the model implicitly assumes that the quantity on the right hand side of Eq. (S1) is positive; when $P < R$, greater values of ε or V_{n} make growth more negative, which would not be expected in real systems.

S1.1 Temperature dependence of P and R

Recent empirical work suggests that photosynthesis and respiration TPCs are typically single-peaked, left-skewed functions of temperature, and well fitted by the Schoolfield-Sharpe model without low-temperature inactivation (4–7):

$$B = \frac{B_0 \exp\left(-\frac{E}{k}\left(\frac{1}{T} - \frac{1}{T_{\mathrm{ref}}}\right)\right)}{1 + \exp\left(\frac{E_{\mathrm{D}}}{k}\left(\frac{1}{T_{\mathrm{h}}} - \frac{1}{T}\right)\right)}. \tag{S6}$$

Here, B is a metabolic rate at a given temperature T (1/day), B_0 is approximately the rate (1/day) at a reference temperature T_{ref} (in K; see ref. 8), E and E_{D} are the activation and de-activation energies (eV) that set the relative rate of increase up to, and decrease from the maximum, respectively, T_{h} is the temperature at which the rate is half inactive due to high temperatures, and $k \approx 8.617 \times 10^{-5}$ eV/K is the Boltzmann constant. The Schoolfield-Sharpe model assumes there is a single rate-limiting enzyme, so while it may be more appropriate to use it to model the temperature dependence of P_{g}, it has also been found to adequately describe P (6; 7). Example P and R TPCs are shown in Fig. 1a in the main text.

S1.2 Temperature dependence of allocation efficiency ε

The dimensionless allocation efficiency ε broadly captures how much available biomass (carbon) is actually translated into cell growth (realised growth, as opposed to the potential growth represented by net flux).

It is important to note that some studies (e.g., refs. 9–11) conflate carbon use efficiency (Section S1.4) and ε, by assuming that the proportion of carbon that is not used in respiration is allocated to growth. Because of storage effects (3; 12), ε can be greater than

one at a given moment in time, but integrated over a sufficiently long time period (e.g., 24 hours or more), ε is expected to be bound between $[0, 1]$.

The temperature dependence of allocation efficiency ε (or mass conversion efficiency in heterotrophs) has been acknowledged (13–19). For instance, one study found (19) found that assimilation efficiencies increased with temperature, another (18) found significant temperature dependence of mass conversion efficiency in two out of six cases in their database, while another study (17) found possible evidence of temperature dependence in several related traits. However, a temperature-dependent allocation efficiency has rarely been incorporated into models of temperature-dependent growth (3; 9; 10; 20–24), and studies have instead often assumed a fixed, temperature-independent ε.

In the main text, we use the Boltzmann-Arrhenius (BA) equation for the TPC of allocation efficiency:

$$\varepsilon = \varepsilon_0 \exp\left(-\frac{E_\varepsilon}{k}\left(\frac{1}{T} - \frac{1}{T_{\text{ref}}}\right)\right), \tag{S7}$$

where normalisation constant ε_0 is the efficiency at T_{ref}, and E_ε sets the relative rate of change of $\varepsilon(T)$ with T. The sign of E_ε determines whether ε increases or decreases with temperature: a positive E_ε suggests that allocation to growth is less efficient at low temperatures, whereas a negative E_ε implies that allocation efficiency drops at higher temperatures, perhaps due to heat stress. There is limited evidence for the temperature dependence of ε over the ecologically relevant "operational" temperature range (OTR) of organisms (16–18); here we make no *a priori* assumption about the directionality of the temperature dependence, and consider both positive and negative values of E_ε (Fig. 1b in the main text). The BA $\varepsilon(T)$ (Eq. S7) allows us to study the effect of putative thermodynamic constraints on the metabolic rates underlying allocation, and is also supported by our experimental data (see Fig. 2c in the main text). We also explore how a quadratic $\varepsilon(T)$,

$$\varepsilon = \alpha + \beta\, T + \gamma\, T^2, \tag{S8}$$

might affect growth rate TPCs (Section S12.3). In this case, the expectation would be $\gamma < 0$ (such that the parabola opens downwards, thus describing a $\varepsilon(T)$ TPC that peaks within the operational temperature range). Here, the maximum ε depends on all parameters while the temperature at which ε is maximised as well as the local rate of change of ε with temperature depend on β and γ. With $\beta = \gamma = 0$, ε becomes independent of temperature.

Mass conservation

Implicit in allocation efficiency ε is the fact that cells lose some of the carbon. Phytoplankton cells commonly exude photosynthetic assimilates instead of storing them or using them for growth (25–30), making them an important contributor to dissolved organic matter (31). Such exudates can account for as much as 77% of total sequestered carbon (29). Moreover, this exudation can happen at timescales (e.g., < 20 minutes; ref. 32) relevant to our theoretical and empirical analyses. Carbon may also be 'lost' if not all processes are accounted for in experimental data on metabolic rates. For example, under certain conditions, alternative (less 'efficient') respiratory pathways may be activated (33; 34), which would complicate any link between the measured use of carbon through respiration, and growth. In terrestrial plants, carbon can further be lost (and thus not available for growth of the population of photosynthetic cells) if it is allocated away from leaves to non-photosynthetic tissues.

S1.3 Temperature dependence of nutrient uptake V_n

Nutrient uptake V_n is also bound between $[0, 1]$. Nutrient limitation affects how net flux translates into cell growth, and scales how much of the available carbon can be used for biosynthesis. The model for nutrient uptake would typically include a term for maximum nutrient uptake rate V_max. The temperature dependence of V_max, according to Aksnes & Egge (35), is equal to the temperature dependence (but opposite sign) of the time it takes a cell to absorb and process a given amount of nutrients. In our model, photosynthesis (and hence also net flux) is assumed to be measured at saturating nutrient concentrations. Therefore, regardless of the true temperature dependence of V_max, what matters here is the temperature dependence of the observed net flux, at saturating nutrient concentrations.

The half-saturation parameter K_S, on the other hand, is expected to increase with temperature (3; 35), and can be phenomenologically modelled as

$$K_S = K_0 \exp\left(\frac{E_K}{k}\left(\frac{1}{T} - \frac{1}{T_\mathrm{ref}}\right)\right). \tag{S9}$$

V_n is expected to be a decreasing function of T (Fig. S1): substituting Eq. (S9) into Eq. (S4), we can show that

$$\frac{\mathrm{d}V_\mathrm{n}}{\mathrm{d}T} = -\frac{S\,\frac{\mathrm{d}K_S}{\mathrm{d}T}}{(K_S + S)^2}. \tag{S10}$$

Given that $E_K > 0$, it follows that $\mathrm{d}K_S/\mathrm{d}T > 0$, and because $K_S > 0$, at low nutrient concentrations, $\mathrm{d}V_\mathrm{n}/\mathrm{d}T < 0$, so V_n decreases with T (Fig. S1).

For a more mechanistic approach to estimating the temperature dependence of nutrient uptake, specific to aquatic autotrophs, see Section S2.

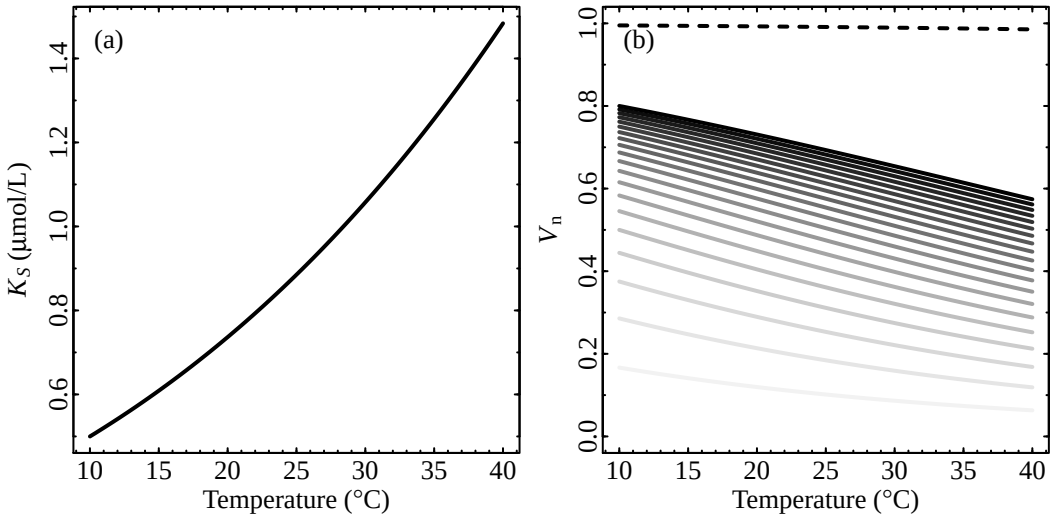

Figure S1: Example temperature dependences of the half-saturation parameter K_S (a) and dimensionless nutrient uptake V_n (b), using $E_K = 0.277$ (3), and arbitrarily setting $K_0 = 0.5$ at $T_\mathrm{ref} = 10°\mathrm{C}$. The lines in (b) correspond to different nutrient concentrations, ranging from 0.1 (light grey) to 2 µmol/L (black), and where the dashed line at $V_\mathrm{n} \approx 1$ corresponds to a nutrient concentration of 100 µmol/L. Note that while this constitutes an example only, if K_S increases with temperature, V_n is expected to decrease with temperature at low enough nutrient concentrations.

S1.4 Carbon use efficiency CUE

Carbon use efficiency (CUE) is frequently used in the literature (e.g., refs. 6; 22; 36) and similarly quantifies a measure of growth potential or metabolic efficiency:

$$\mathrm{CUE} = 1 - \frac{R}{P_\mathrm{g}} = \frac{P}{P_\mathrm{g}}, \tag{S11}$$

although CUE is sometimes defined differently (11). Because P_g and R_l are not typically independently measured in experiments, estimating CUE usually requires the assumption that $R \approx R_\mathrm{l}$, and thus that $P_\mathrm{g} \approx P + R$. CUE is reportedly constrained and the target of selection (6; 36), which points to the interdependence of the metabolic rates. Respiration depends on P_g for substrate, while P_g relies on respiration for a range of compounds (e.g., ATP), and growth in turn is contingent on both P_g and respiration (11; 37). These links are not explicit in the model of Eq. (S1) or many others like it, because models assume carbon limitation only. A constrained CUE does not necessarily, however, constrain net flux (which should more directly relate to population growth rate; Eq. S1); variation in net flux (and growth rate) should still be possible with a fixed CUE. In an evolutionary context, this also means that up (7) or down-regulation (6) of both P and R can lead to changes in net flux while keeping CUE relatively constant.

The temperature dependence of CUE is defined by the temperature dependences of the underlying rates, and therefore, systematic differences in the Schoolfield-Sharpe parameters for P and R will determine how CUE changes as a function of temperature (Section S3; ref. 6).

S1.5 Comparison with previously published models

Our model resembles and is analogous to some previously published models, (e.g., refs. 38; 39). Amthor (38) builds on work by Thornley (40) among others and in his Eq. (8) describes the growth of dry biomass W (in units of g CO_2 equivalents per unit area) over time t as

$$\frac{\Delta W}{\Delta t} = Y_G\,(P - m\,W) \tag{S12}$$

$$= Y_G \left(\frac{\Delta S}{\Delta t} - \frac{\Delta S_M}{\Delta t}\right), \tag{S13}$$

with the 'true growth yield'

$$Y_G = \frac{\Delta S_T}{\Delta S_R + \Delta S_T}. \tag{S14}$$

In their model, P is "gross photosynthesis (less photorespiration)", equivalent to our net photosynthesis P, ΔS is the total substrate generated by photosynthesis, which is

$$\Delta S = P\,\Delta t = \Delta S_T + \Delta S_M + \Delta S_R, \tag{S15}$$

ΔS_T is the 'carbon skeleton' that becomes new plant material (i.e., analogous to our r), ΔS_M is maintenance respiration, ΔS_R is the respiration associated with generating energy necessary for growth, and thus total respiration

$$R\,\Delta t = \Delta S_M + \Delta S_R. \tag{S16}$$

Eq. (S15) can be re-arranged to give

$$\Delta S_T = \Delta S - \Delta S_M - \Delta S_R$$

$$= (P - R)\,\Delta t. \tag{S17}$$

The similarity of this model with ours is evident, although Amthor (38) explicitly unpacks respiration into two separate components (maintenance and biosynthesis respiration). His approach suggests that allocation efficiency ε might include elements of the respiratory pathway that are associated with biosynthesis (e.g., ΔS_R), but not fully captured by measurements of our P and R.

Thomas *et al.* (39) use a more general approach, the 'double exponential model', which they define in their Eq. (3) as

$$\mu = b_1 \exp(b_2\, T)\, \frac{R}{R+K} - (d_0 + d_1 \exp(d_2\, T)), \tag{S18}$$

where μ is our r, R is our S (the nutrient concentration), and K is our K_S (the half-saturation parameter). The two exponential terms correspond to a reproduction/birth (anabolic) rate and a mortality (catabolic) rate respectively. When applying the model to autotrophs, the two exponential terms are analogous to photosynthesis (the rate at which carbon is fixed) and respiration (the rate at which carbon is consumed and therefore not available for growth), respectively. Nutrient limitation here only affects the anabolic term. This model resembles our alternative model structure (Model II in Section S9), with the only difference of the d_0 parameter, missing in our version of the model.

S2 Mechanistic model of nutrient uptake in aquatic autotrophs

Temperature is expected to affect nutrient uptake through maximum nutrient uptake rate $V_{\max}$ (14; 15; 41) and K_S (3; 35). In the models of Eqs. (S35)–(S37), the effect of temperature on $V_{\max}$ is implicit in the temperature dependence of net flux. The temperature dependence of K_S has proven to be ambiguous in experiments (2; 41), and difficult to interpret biologically. In fact, temperature is often assumed to only affect maximum nutrient uptake alone (14; 15). Mechanistic models of nutrient uptake necessary for understanding the temperature dependence of K_S exist (35; 42–45). In the derivation of Aksnes & Egge (35), a cell is assumed to have a number of uptake sites of average area A (m^2), in which nutrient ions are absorbed and processed at a rate h (µmol nutrients/hr). In their model,

$$K_S = \frac{1}{A\, v\, h}, \tag{S19}$$

and v, the mass-transfer coefficient (m/hr), expresses the relative velocity between nutrient ions and the cell:

$$v = \frac{D}{r_\mathrm{c}} + \frac{u}{2}. \tag{S20}$$

Here u is the relative velocity between the cell and the medium (m/hr), r_c is the radius of the cell (m), and D is the diffusion coefficient (m^2/hr). The Stokes-Einstein equation relates diffusion to temperature:

$$D = \frac{k\, T}{6\, \pi\, \eta\, r} \tag{S21}$$

(3), where η is the dynamic viscosity of the medium (kg/(hr·m)), and r is the radius of the nutrient ion. We know that η and h decrease exponentially with temperature, so

$$\eta = B_\eta \exp\left(\frac{E_\eta}{k\, T}\right), \text{and} \tag{S22}$$

$$h = B_h \exp\left(\frac{E_h}{k\, T}\right). \tag{S23}$$

Some phytoplankton species have evolved means to move in the medium (e.g., flagella). Flow around organisms is determined by the Reynolds number (Re), which is a dimensionless quantity defined as the ratio of inertial forces to viscous forces. For phytoplankton, $\mathrm{Re} \ll 1$ (46), meaning that flow is dominated by viscous forces, and fully laminar. In these cases, Stokes' law can be used to derive velocity u:

$$F = 6\,\pi\,\eta\,r_{\mathrm{c}}\,u, \tag{S24}$$

where F is the drag force experienced by the cell (N). Stokes' drag assumes that the cells have smooth surfaces, and that there is no interference between cells. The power required to overcome F and move the cell through the fluid at velocity u is $P = F\,u$ (J/hr; ref. 47). Therefore, u can be determined from the power available to the cell, which could be assumed to be proportional to the respiration rate R of the cell (in units of J/hr). Therefore,

$$u = \sqrt{\frac{\zeta\,R}{6\,\pi\,\eta\,r_c}}, \tag{S25}$$

where ζ is the proportion of the energy produced in R allocated to propulsion. The temperature dependence of u is

$$u \propto \frac{\exp\left(\dfrac{-(E_R + E_\eta)}{k\,T}\right)}{1 + \exp\left(\dfrac{E_{\mathrm{D},R}}{k}\left(\dfrac{1}{T_{\mathrm{h}}} - \dfrac{1}{T}\right)\right)}. \tag{S26}$$

Assuming $u \approx 0$, the temperature dependence of K_S would be

$$K_S \propto \frac{1}{T\,\exp\left(\dfrac{E_h - E_\eta}{k\,T}\right)}, \tag{S27}$$

whereas including u adds an extra term in the denominator.

The effect of u on the sensitivity of K_S to an increase in temperature will be driven by the temperature dependence of R. When R increases (respectively decreases) with T, the sensitivity of K_S will be reduced (respectively increased) relative to when $u \approx 0$.

The dynamic viscosity of water decreases with temperature. Reuman *et al.* (3) found that $E_\eta = 0.1781$ and $B_\eta = \exp(-13.8738)$ at a reference temperature of 20°C. They also conducted an interspecific meta-analysis to estimate the activation energy of K_S, from which they found that $E_K = 0.217$, and together with E_η (using eq. S27), deduced that $E_h = 0.456$. Because $E_K > 0$, K_S increases with temperature, and thus, nutrient uptake at a given nutrient concentration decreases with temperature (e.g., Fig. S1).

S3 Effect of the temperature dependence of P and R on the net flux TPC

The growth rate TPC depends on that for net flux F, which in turn consists of the difference in the TPCs of photosynthesis and respiration. Even if we let P and R be described by exponential (Boltzmann-Arrhenius) functions within a given (inverse, $1/kT$) operational temperature range, the difference between P and R can produce a wide range of qualitatively different net flux TPCs. Let

$$\begin{aligned} F &= P - R, \\ &= P_0 \exp\left(-\frac{E_P}{k}\left(\frac{1}{T} - \frac{1}{T_{\text{ref}}}\right)\right) - R_0 \exp\left(-\frac{E_R}{k}\left(\frac{1}{T} - \frac{1}{T_{\text{ref}}}\right)\right). \end{aligned} \tag{S28}$$

F, P, and R are assumed to be rates in units of 1/day. Taking the derivative of F with respect to T,

$$\frac{\mathrm{d}F}{\mathrm{d}T} = \frac{E_P\, P_0}{k\, T^2} \exp\left(-\frac{E_P}{k}\left(\frac{1}{T} - \frac{1}{T_{\text{ref}}}\right)\right) - \frac{E_R\, R_0}{k\, T^2} \exp\left(-\frac{E_R}{k}\left(\frac{1}{T} - \frac{1}{T_{\text{ref}}}\right)\right). \tag{S29}$$

This derivative is the sensitivity of net flux to a unit increase in temperature, at temperature T, and consists of the difference in the sensitivities of photosynthesis and respiration to increases in temperature. Therefore, if both P and R are equally sensitive to an increase in temperature, the resultant net flux would be insensitive to temperature at T. Similarly, both P and R can be highly sensitive to increases in temperature, but if the difference in their sensitivities is small, net flux would only be marginally sensitive to temperature. Solving for T at $\mathrm{d}F/\mathrm{d}T = 0$ yields

$$T_{\text{pk},F} = \frac{E_P - E_R}{k\left[\ln\left(\frac{E_P}{E_R}\,\frac{P_0}{R_0}\right) - \frac{E_R - E_P}{k\, T_{\text{ref}}}\right]}, \tag{S30}$$

the temperature for maximum net flux. Therefore, while in this example both P and R monotonically increase with temperature, the net flux TPC can be single peaked (Figs. S2 and S3).

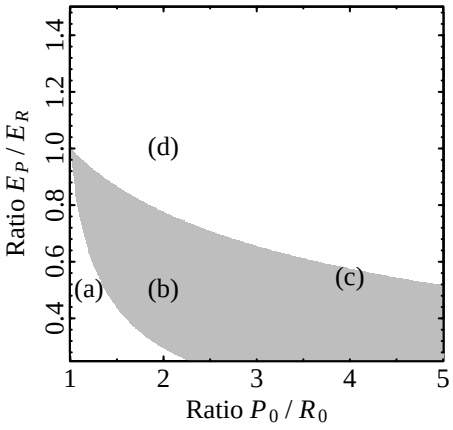

Figure S2: Parameter combinations that yield a $T_{\text{pk},F}$ within $0 < T < 40$°C are shown in grey. In this example, $R_0 = 1$ and $E_R = 0.5$. The letters point to panels in Fig. S3, where example net flux TPCs for those parameter combinations are shown.

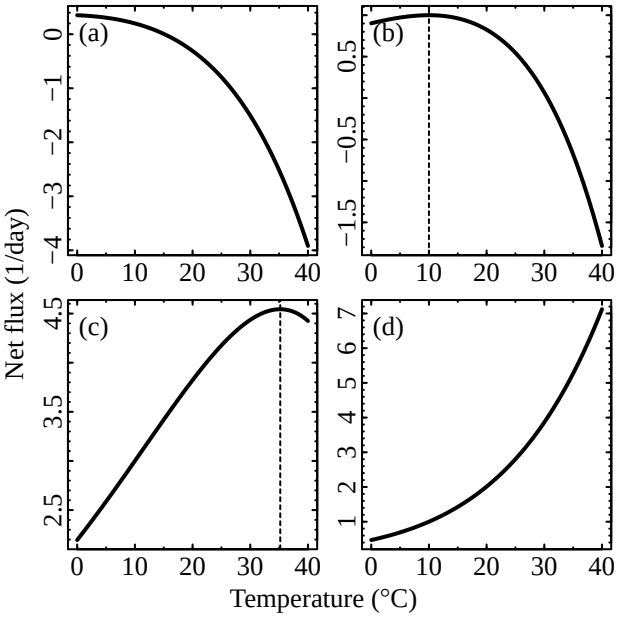

Figure S3: Example growth TPCs for four example parameter combinations shown in Fig. S2. Vertical lines denote the temperature at which maximum growth is achieved, when within the temperature range.

S4 Describing the growth rate TPC

Several parameters are widely used in the literature to describe different aspects of the growth rate TPC, including the critical thermal minimum and maximum (the lower and upper temperatures between which growth rates are positive; refs. 39; 48; 49), the relative rate of increase of growth rate with temperature (estimated, for instance, as an activation energy; refs. 7; 17; 24; 50; 51), and the temperature at which growth rate is maximised ($T_{\mathrm{pk},r}$; refs. 39; 52; 53). Empirical evidence indicates that the biologically most relevant OTR is likely to comprise the rising part of the growth rate TPC up to, approximately, its maximum (54). One possible explanation for this relies on Jensen's inequality: contingent on the variability of the local environment, organisms' fitness may be expected to be optimised at mean temperatures below the temperature of maximum growth $T_{\mathrm{pk},r}$ (55–57). The most relevant descriptors for growth within the OTR are therefore the relative rate of change of growth to increases in temperature, and $T_{\mathrm{pk},r}$. Although the former is often estimated by fitting the Boltzmann-Arrhenius equation (or elaborations thereof; e.g., Eq. S6) to the growth rate TPCs (7; 50; 51), it is important to emphasise that growth rates in autotrophs are driven by multiple metabolic processes, thereby likely violating the models' assumption of a single rate-limiting enzyme. However, we will still refer to the "activation energy of growth" (E_r) to describe the relative rate of increase of growth rates up to $T_{\mathrm{pk},r}$.

S5 Effect of $\varepsilon(T)$ on the activation energy of growth rate E_r

By describing the relative rate of increase of growth rates with temperature (i.e., E_r from Eq. S7), we (and studies that follow this approach) implicitly assume that growth rates increase exponentially for $1/(k\,T) > 1/(k\,T_{\mathrm{pk},r})$. In this temperature range, metabolic rates are likely adequately described by the Boltzmann-Arrhenius model (the numerator of Eq. S6). We can take a first order Taylor approximation of ln growth rate (Eq. S1) around $1/(k\,T_{\mathrm{ref}})$, which yields

$$\ln r \approx \ln(\varepsilon(T = T_{\mathrm{ref}})) + \ln(P_0 - R_0) + \left[\frac{\frac{\mathrm{d}\varepsilon}{\mathrm{d}x}(T = T_{\mathrm{ref}})}{\varepsilon(T = T_{\mathrm{ref}})} + \frac{P_0\,E_P - R_0\,E_R}{P_0 - R_0}\right]\left(x - \frac{1}{k\,T_{\mathrm{ref}}}\right), \tag{S31}$$

where $x = 1/(k\,T)$. On linear scales, this corresponds to the Boltzmann-Arrhenius equation. The term in square brackets corresponds to the slope of $\ln r$ with $x = 1/(k\,T)$, and is thus the approximate activation energy of growth rate:

$$E_r \approx \frac{\frac{\mathrm{d}\varepsilon}{\mathrm{d}x}(T = T_{\mathrm{ref}})}{\varepsilon(T = T_{\mathrm{ref}})} + \frac{P_0\,E_P - R_0\,E_R}{P_0 - R_0}. \tag{S32}$$

The first term of Eq. (S32) represents the effect of $\varepsilon(T)$ on E_r (it is otherwise zero when ε is independent of T). For example, for the BA-form of $\varepsilon(T)$ (Eq. S7), Eq. (S32) becomes

$$E_r \approx E_\varepsilon + \frac{P_0\,E_P - R_0\,E_R}{P_0 - R_0}, \tag{S33}$$

so E_ε represents the change in E_r due to $\varepsilon(T)$ (ΔE_r in the main text). Note that the normalisation constant ε_0 has no effect on how $\varepsilon(T)$ alters the temperature dependence of growth. For a quadratic $\varepsilon(T)$ (Eq. S8),

$$E_r \approx -\frac{k\,(\beta\,T_{\mathrm{ref}}^2 + 2\,\gamma\,T_{\mathrm{ref}}^3)}{\alpha + \beta\,T_{\mathrm{ref}} + \gamma\,T_{\mathrm{ref}}^2} + \frac{P_0\,E_P - R_0\,E_R}{P_0 - R_0}. \tag{S34}$$

Here, the effect of $\varepsilon(T)$ on E_r is more complicated and contingent on the values of α, β, and γ.

S6 Example parameterisations for $\varepsilon(T)$

To illustrate the effects of a temperature dependent $\varepsilon(T)$ on potential exponential growth rates, we use a very diverse dataset covering many species from various locations and including a wide range of different temperature ranges. The allocation efficiency $\varepsilon(T)$ could be expected to vary significantly across different species, but in our analysis, we use the same parameterisations across all species. We use two main forms of temperature dependence of $\varepsilon(T)$, the BA-form (Eq. S7), which we focus on in the main text, and the quadratic (Eq. S8). To assess the robustness of our results to the parameterisation of $\varepsilon(T)$, we use two different approaches for each form of $\varepsilon(T)$.

S6.1 Boltzmann-Arrhenius $\varepsilon(T)$

We explicitly change activation energy E_ε (Eq. S7) to assess how the strength of the temperature dependence of ε affects the potential growth rate TPC. We use a maximum $|E_\varepsilon|$ that is close to that found in the laboratory experiments ($|E_\varepsilon| = 0.65$ eV; Fig. 2 in the main text). We then use two different constraints to parameterise the normalisation constant ε_0): (i) the overall performance loss between T_{min} and $T_{\text{pk},P}$ is 50% (used in the main text; Fig. S4a); and (ii) $\varepsilon(T = T_{\text{pk},P}) = 0.5$ (Fig. S4b).

S6.2 Quadratic $\varepsilon(T)$

We explicitly set the curvature ω of the quadratic function (Eq. S8), to assess how the strength of the temperature dependence of $\varepsilon(T)$ affects the potential growth rate TPC. We use a maximum $|\omega|$ the ensures that within the relevant temperature range, $0 \leq \varepsilon(T) \leq 1$. As with the BA-form, we use two different sets of constraints to parameterise α and β: (i) $\varepsilon(T)$ peaks at the midpoint between T_{min} and $T_{\text{pk},P}$ and overall performance loss between T_{min} and $T_{\text{pk},P}$ is set to 50% (Fig. S4c); and (ii) $\varepsilon(T)$ peaks at $T_{\text{pk},P}$, and $\varepsilon(T = T_{\text{pk},P}) = 0.7$ (Fig. S4d).

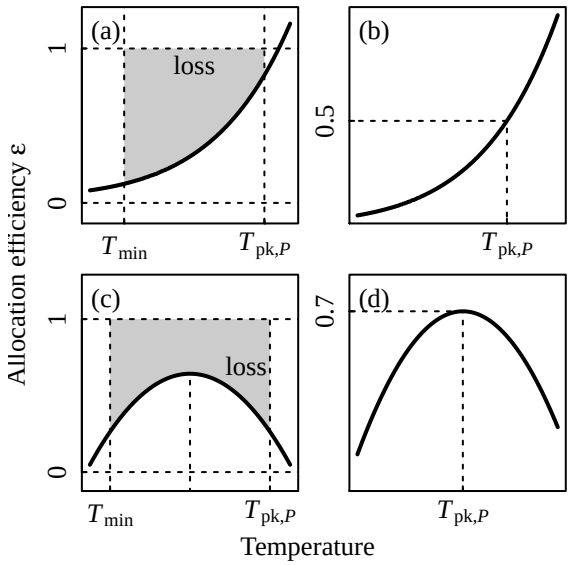

Figure S4: Illustrations of the constraints used to produce example parameterisations for the BA-form (a,b) and quadratic (c,d) $\varepsilon(T)$. Note that in (c) ε peaks at the midpoint between T_{min} and $T_{\text{pk},P}$. We use the constraints depicted in (a) to parameterise the $\varepsilon(T)$ functions used in the main text, and show additional results for parameterisations in (b–d) in Figs. S9–S13.

S7 Fitting response functions to simulated growth data

The potential growth rate TPCs could sometimes be negative (if net flux was negative at high temperatures), or equal to zero (at either temperature extreme). To estimate the activation energy of the growth rate TPC we fit the Schoolfield-Sharpe model to the ln growth rates; for the purpose of fitting, the negative values needed to be removed. However, even very small growth rates caused the fits to be problematic: the ln of very small values can be large negative values, and therefore the fit could be increasingly driven by these points. Because we were interested in the rise of the curve with temperature, but less so in its decline after $T_{\mathrm{pk},r}$, for fitting the model to the data, we removed growth rates at high temperatures whenever $r < (r_{\max}/2)$. We also excluded any growth rates $r < 0.02$ to avoid very small values at low temperatures.

S8 Activation energy of potential growth rates E_r as a function of the operational temperature range

For some species, when the BA-form of $\varepsilon(T)$ with $E_\varepsilon < 0$ (Eq. S7) is applied, the resulting growth rate TPC can have a peak close to the minimum experimental range. For example, for *Cladophora glomerata*, the peak growth with temperature-independent $\varepsilon(\kappa)$ is 14.2°C, while with $E_\varepsilon = -0.32$ eV, peak growth is at 3.2°C. For this species, the minimum experimental temperature (with measurements for both P and R) was 0°C, which leaves 3.2°C over which to estimate the activation energy of growth rates. In normal circumstances, this is the range over which E_r would be estimated (and for this reason we follow this approach in our analysis in the main text). This estimate is, however, likely lower than the activation energy that would be estimated, were the growth curve to be extrapolated down to lower temperatures. To illustrate this, we show the growth curve for the example mentioned above in Fig. S5, and how the activation energy changes as the temperature range over which it is estimated increases (via extrapolation of the growth curve). Here, the change in E_r is very limited.

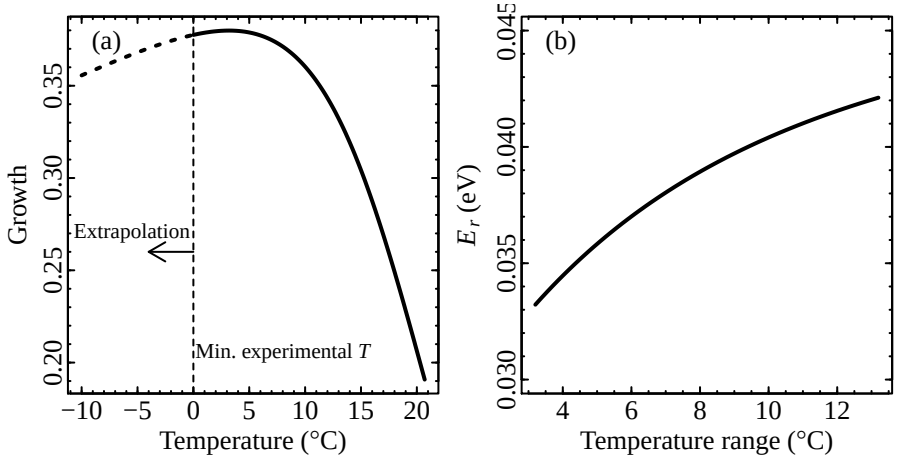

Figure S5: (a) Growth rate TPC for *Cladophora glomerata* with a temperature dependent $\varepsilon(T)$ with $E_\varepsilon = -0.32$ eV. The solid line is the part of the potential growth curve that lies within the experimental temperature range, while the dashed line is an extrapolation, using the Schoolfield-Sharpe parameters for P and R, and extrapolating the $\varepsilon(T)$ curve. (b) Activation energy of the potential growth rate E_r estimated using different ranges of temperature, from a value of 3.2°C (the range between the minimum experimental temperature and temperature at maximum growth), and increasing the temperature range by extrapolation.

S9 Alternative model structures

While in the main text and in Section S1 we develop a model structure that most closely mirrors those developed in previous studies, there are also potentially valid alternative formulations:

$$\frac{1}{N}\frac{\mathrm{d}N}{\mathrm{d}t} = r = \varepsilon\, V_\mathrm{n}\,(P_\mathrm{g} - R_\mathrm{l} - R), \qquad \text{Model I} \tag{S35}$$

$$r = \varepsilon\, V_\mathrm{n}\, P_\mathrm{g} - R_\mathrm{l} - R, \qquad \text{Model II} \tag{S36}$$

$$r = \varepsilon(V_\mathrm{n}\, P_\mathrm{g} - R_\mathrm{l} - R). \qquad \text{Model III} \tag{S37}$$

(where we focus on Model I). The meaning of the allocation efficiency $\varepsilon(T)$ subtly depends on the model formulation; in Models I and III, it captures how much biomass (carbon) available (after accounting for respiration) is translated into growth, while in Model II it represents how much of the carbon fixed (without accounting for respiration) is used in growth. Similarly, the meaning of nutrient limitation depends on model formulation; in Model I, a lack of nutrients affects how net flux translates into cell growth, whereas in Models II and III, a lack of nutrients affects a cell's ability to fix carbon.

We fit Models I and II to the case study data ($V_\mathrm{n} \approx 1$ so Model I = Model III), and use AIC to select the most likely model structure given the data.

S10 Laboratory experiments on *Chlorella vulgaris*

We use laboratory experiments on *Chlorella vulgaris*, to infer the most likely population model structure and temperature dependence of $\varepsilon(T)$, as well as to explore evolutionary implications of our results. Full details on the experimental setup can be found in ref. (6). *C. vulgaris* cells were isolated from a pond in northern England 15 years ago, and have since been maintained at 20°C. Three replicate populations of *C. vulgaris* were established per five different growth temperatures (20, 23, 27, 30, and 33°C) under nutrient and light saturated conditions, and kept in their exponential growth phase. Maximum growth rates for each growth temperature were estimated by fitting the logistic growth curve,

$$N_t = \frac{K}{1 + \dfrac{K - N_0}{N_0}\, e^{-r_\mathrm{max}\, t}}, \tag{S38}$$

to biomass trajectories measured after approximately 10 ("acclimated") and 100 ("adapted") generations. Here, r_max is the maximum exponential growth rate, K is the carrying capacity, N_0 the starting population density, and N_t the population density at time t. Padfield *et al.* (6) also measured the acute short-term responses of metabolic rates (net photosynthesis P and dark respiration R) to temperatures between 10 and 49°C for each of the populations grown at the five growth temperatures, both after 10 and 100 generations. Net photosynthesis and respiration were estimated by measuring the rates of change of oxygen concentration in the light and dark, respectively. P was estimated at light intensities that maximised photosynthetic rates. Both metabolic rates were mass-normalised by dividing the rates by the biomass estimated in each experiment.

Acute responses of metabolic rates to a change in temperature are typically measured in brief (order of minutes) experiments in stressful conditions for the cells. On the other hand, growth rate experiments take longer (order of days), to ensure maximum exponential growth rates are captured. To allow the most direct comparison between metabolic rates

and growth rates, we needed acclimated and adapted responses of metabolic rates. We fitted the Schoolfield-Sharpe model (Eq. S6) to each acute response, and used the model to estimate the metabolic rates at the culture's corresponding growth temperature (i.e., we estimated P and R at 20°C for the cultures acclimated and adapted to 20°C, at 23°C for the cultures grown at 23°C, and so on; Fig. S6). When fitting the models to the data we averaged metabolic rates and growth rates across the three replicates. As a result, we had experimental values of P, R, and growth rates, for both acclimated and adapted responses.

Because experiments were undertaken under nutrient saturated conditions, a simplified version of the above model is used, where $V_{\mathrm{n}} \approx 1$. For the alternative model structure (Section S9) we assume that $P_{\mathrm{g}} \approx P + R_{\mathrm{l}}$, and that $R \approx R_{\mathrm{l}}$.

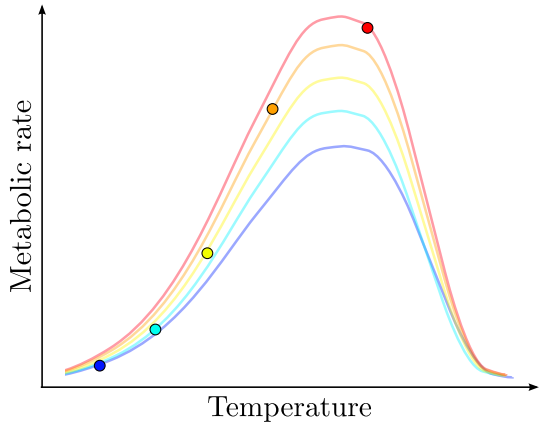

Figure S6: Illustration of how the acclimated and adapted responses of metabolic rates to temperature were estimated in the experiments of Padfield *et al.* (6). The coloured lines represent the acute responses of metabolic rates to changes in temperature, and each colour corresponds to a different growth temperature. Schoolfield-Sharpe models were fit to the acute responses, and using these models, the metabolic rates at the corresponding growth temperature were estimated (i.e., at the points at which acute experimental temperature equalled growth temperature), thus producing one metabolic rate per growth temperature.

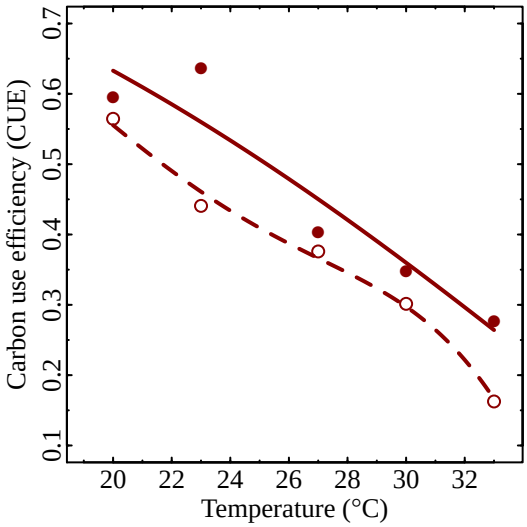

Figure S7: Carbon use efficiency for acclimated populations (dashed line and hollow points) and adapted populations (solid line and points).

S11 Model fits

Table S1: AIC values for model fits to data. The models of Eqs. (S35)–(S37) were fit to the data using nonlinear least squares with a temperature independent $\varepsilon(\kappa)$, and a BA-form $\varepsilon(T)$, separately for acclimated and adapted responses. We here assume $V_{\mathrm{n}} \approx 1$, such that Model I = Model III. There is clear support for Models I & III, and for the BA-form of $\varepsilon(T)$ over $\varepsilon(\kappa)$.

	Models I & III	*Model II*
Acclimated response		
Constant $\varepsilon(\kappa)$	10.6	28.5
BA $\varepsilon(T)$	5.1	13.4
Adapted response		
Constant $\varepsilon(\kappa)$	16.2	25.2
BA $\varepsilon(T)$	8.5	15.4

Table S2: Parameter estimates from the model fits of Table S1, with standard errors in parentheses. Parameters correspond to those of Eqs. (S7) and (S8).

		Models I & III	*Model II*
Acclimated response			
Constant $\varepsilon(\kappa)$	κ	0.202 (0.028)	0.385 (0.027)
BA $\varepsilon(T)$	ε_0	0.059 (0.025)	0.340 (0.033)
	E_ε	0.528 (0.169)	0.311 (0.035)
Adapted response			
Constant $\varepsilon(\kappa)$	κ	0.291 (0.069)	0.376 (0.033)
BA $\varepsilon(T)$	ε_0	0.068 (0.033)	0.342 (0.060)
	E_ε	0.636 (0.179)	0.302 (0.063)

S12 Additional results

S12.1 Results for combined terrestrial and aquatic species

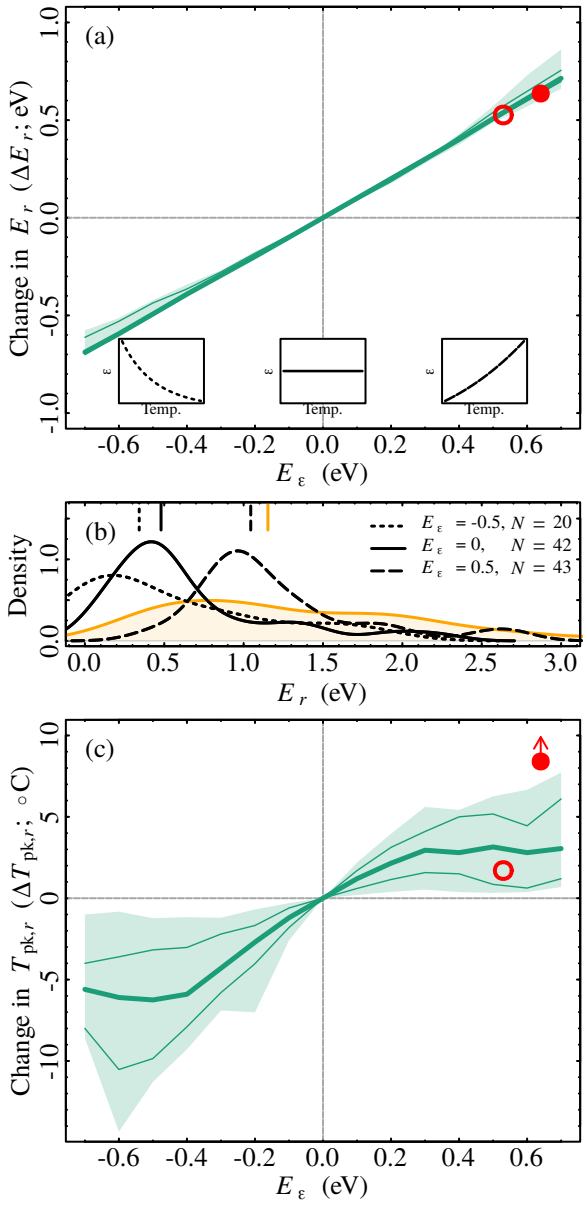

Figure S8: As in Fig. 4 in the main text, but using data for both aquatic and terrestrial species combined (a total of 43 pairs of photosynthesis and respiration curves). The patterns do not differ qualitatively from those in aquatic species only (Fig. 4 in the main text).

S12.2 Alternative parameterisation of the Boltzmann-Arrhenius $\varepsilon(T)$

To assess the robustness of our results, we repeated the analysis (here including both terrestrial and aquatic species, as in Fig. S8 above) with an alternative parameterisation of ε_0 (Eq. S7; Section S6). The results are shown in Fig. S9. The pattern in ΔE_r remains unchanged, as expected (Section S5); the change in E_r due to $\varepsilon(T)$ corresponds to E_ε (compare Fig. 4a in the main text and Fig. S8a to Fig. S9a). For $\Delta T_{\mathrm{pk},r}$, the pattern is qualitatively similar ($\Delta T_{\mathrm{pk},r}$ and E_ε are correlated), but differs quantitatively (compare Fig. 4c in the main text and Fig. S8c to Fig. S9c). Changes in $T_{\mathrm{pk},r}$ are contingent on both the shapes of the underlying P and R TPCs, and ε_0.

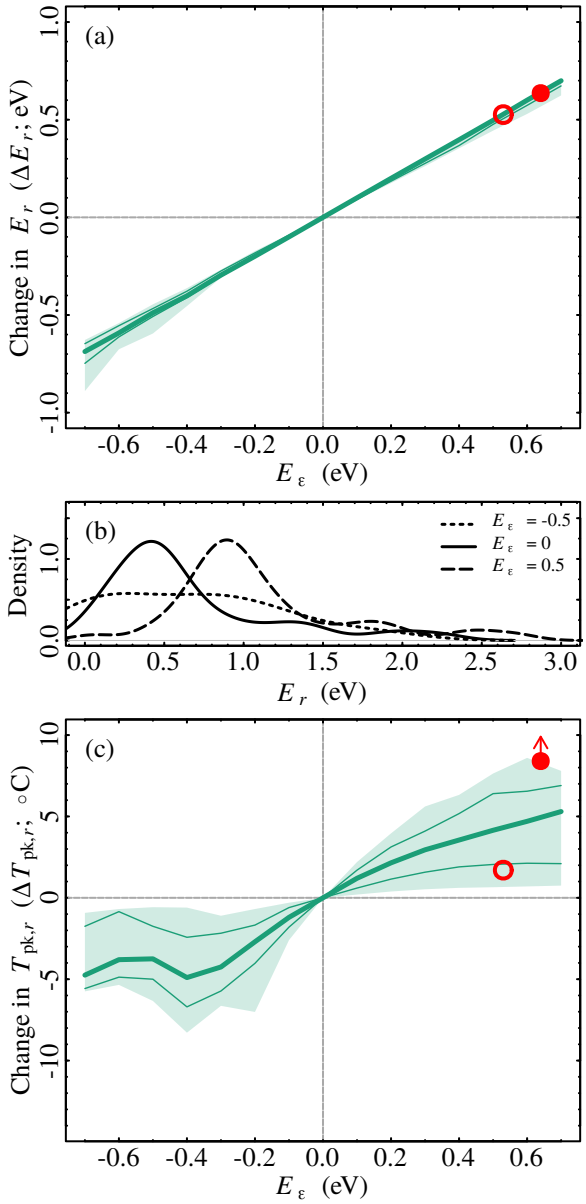

Figure S9: As in Fig. S8, but with the alternative parameterisation of the BA form of $\varepsilon(T)$ (Fig. S4b).

S12.3 Quadratic form of allocation efficiency $\varepsilon(T)$

In the main text we focus on the BA $\varepsilon(T)$. We also explored the scenario where $\varepsilon(T)$ peaks within the OTR, as opposed to being a monotonic function of temperature. To do this, we used a quadratic function, assuming $\gamma < 0$ (Eq. S8; Section S6). Fig. S10 is analogous to Fig. 1 in the main text, but with the quadratic function parameterised as in Fig. S4c. In this parameterisation, $\varepsilon(T)$ peaks at the midpoint between the minimum temperature, and $T_{\mathrm{pk},P}$, meaning that the temperature dependence of $\varepsilon(T)$ over the OTR is relatively limited (Fig. S10b). For this reason, the effect of $\varepsilon(T)$ on E_r is also limited (Fig. S10d). Around $T_{\mathrm{pk},F}$, $\varepsilon(T)$ decreases with temperature (Fig. S10b), and as a result, $T_{\mathrm{pk},r}$ is lowered ($\Delta T_{\mathrm{pk},r} < 0$; Fig. S10e). These patterns are broadly maintained across aquatic and terrestrial species (Fig. S11).

In the alternative parameterisation of the quadratic $\varepsilon(T)$ (Fig. S4d), $\varepsilon(T)$ peaks at $T_{\mathrm{pk},P}$ - roughly the upper limit of the OTR. As a result, $\varepsilon(T)$ increases with temperature over the OTR, although is different in shape to the BA $\varepsilon(T)$ (its second derivative is of the opposite sign). The effect of $\varepsilon(T)$ on ΔE_r is here more substantial (Figs. S12d) and comparable to the impact of the BA $\varepsilon(T)$ (Figs. 1d and 4a in the main text). As expected by the theory (Section S5), ΔE_r here depends on all parameters of the quadratic function. Parameters α and β (Eq. S8) differ between populations, so while the effect of $\varepsilon(T)$ on ΔE_r is qualitatively consistent (a greater curvature γ makes potential growth rates more sensitive to T), how much E_r changes by depends on the population (see the wide shaded areas of S13a). Conversely, $\varepsilon(T)$ is relatively temperature insensitive around $T_{\mathrm{pk},F}$, meaning that its effect on $T_{\mathrm{pk},r}$ is very limited (Figs. S12e and S13c).

In summary, the degree to which $\varepsilon(T)$ affects E_r and $T_{\mathrm{pk},r}$ depends on the temperature dependence of $\varepsilon(T)$ throughout the OTR and around $T_{\mathrm{pk},F}$, respectively. For example, if $\varepsilon(T)$ is temperature-dependent over the rising part of the net flux curve, but relatively temperature insensitive around $T_{\mathrm{pk},F}$, then ΔE_r will be significant while $\Delta T_{\mathrm{pk},r}$ will be small (e.g., Fig. S12). On the other hand, if $\varepsilon(T)$ is temperature-dependent throughout the OTR, including around $T_{\mathrm{pk},F}$, then both ΔE_r and $\Delta T_{\mathrm{pk},r}$ will be significant (as is the case with the BA $\varepsilon(T)$; Figs. 1 and 4 in the main text).

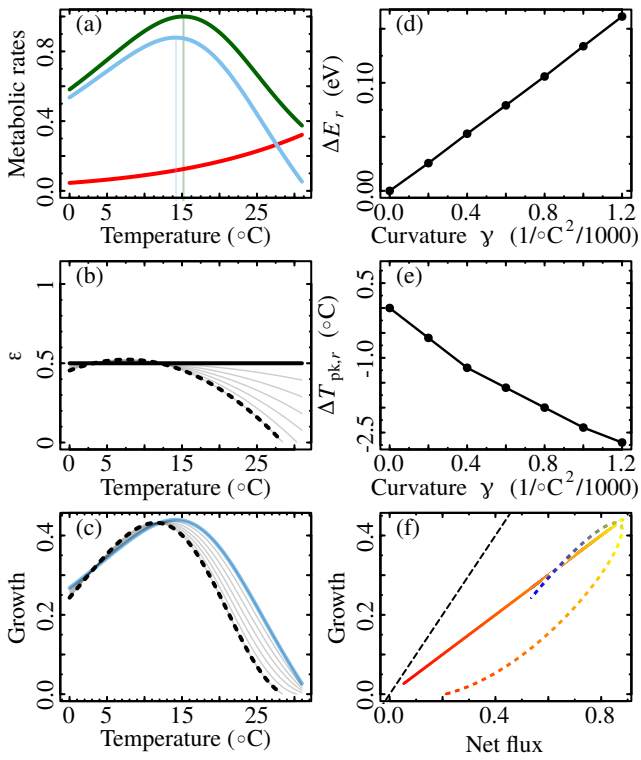

Figure S10: As in Fig. 1 in the main text, but with the quadratic form of $\varepsilon(T)$ (Fig. S4c).

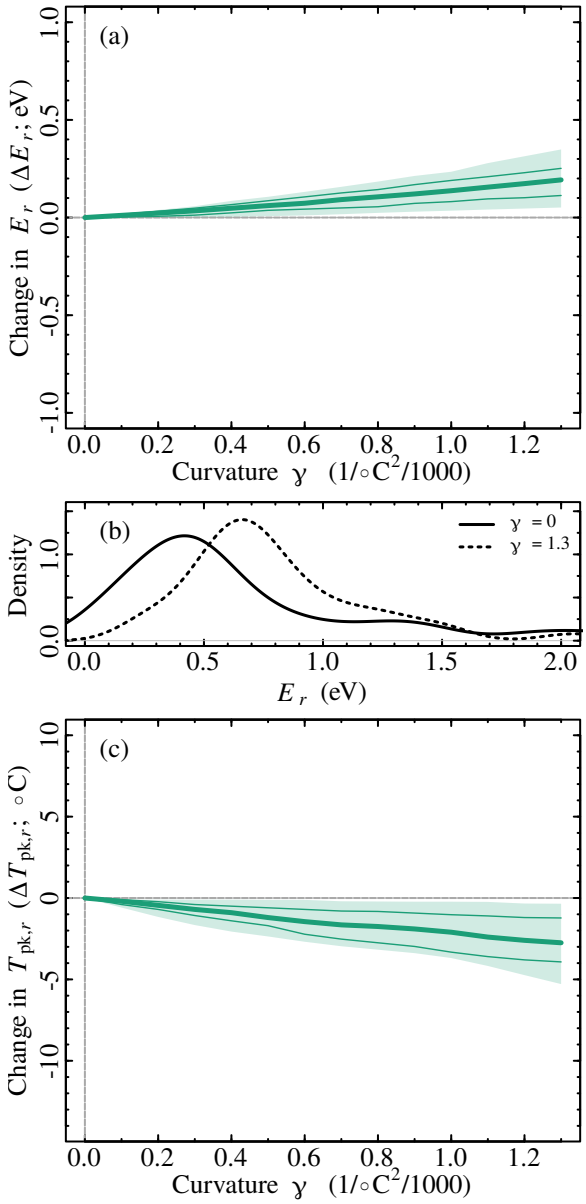

Figure S11: As in Fig. S8, but with the quadratic form of $\varepsilon(T)$ (Fig. S4c).

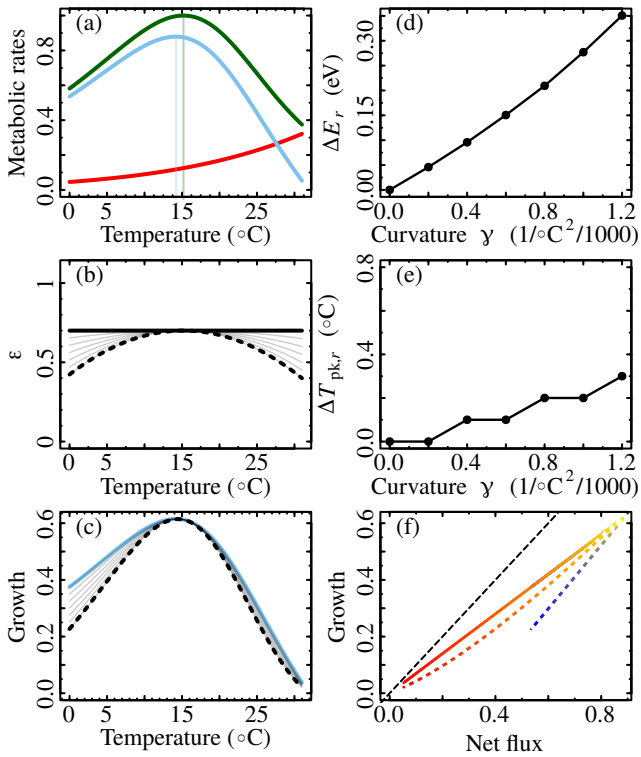

Figure S12: As in Fig. 1 in the main text, with the alternative parameterisation for the quadratic form of $\varepsilon(T)$ (Fig. S4d).

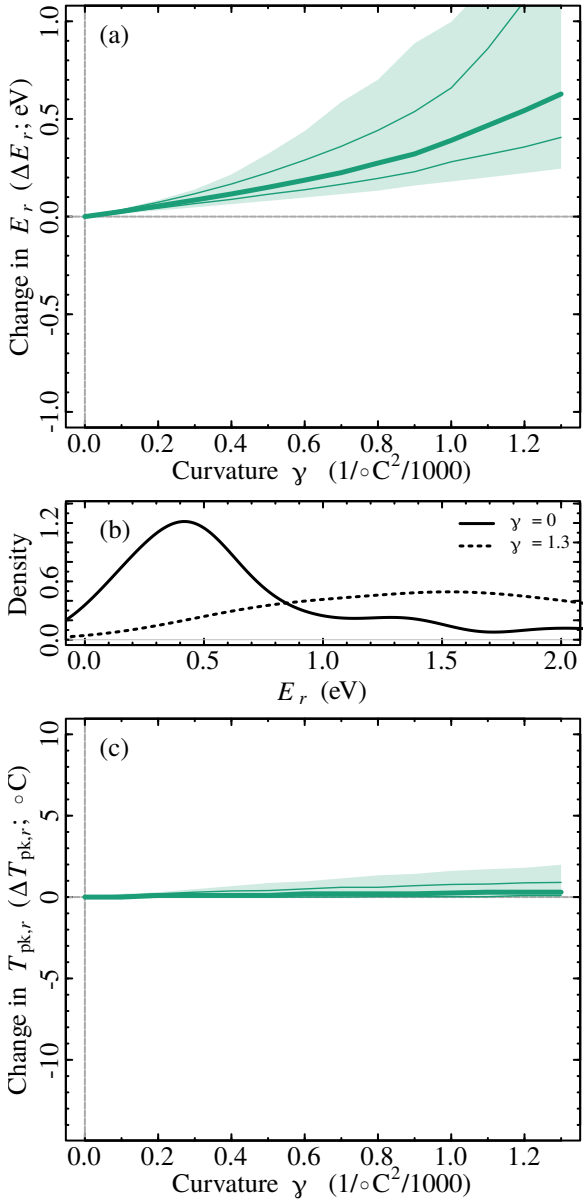

Figure S13: As in Fig. S8, but with the alternative parameterisation of the quadratic form of $\varepsilon(T)$ (Fig. S4d).

S12.4 Nutrient limitation

Nutrient uptake V_{n} is expected to decrease with temperature (Section S1.3). Its effect on potential growth rates is therefore expected to be analogous to an $\varepsilon(T)$ that decreases with temperature (e.g., the BA $\varepsilon(T)$ with $E_\varepsilon < 0$). Fig. S14 confirms this expectation: both E_r and $T_{\mathrm{pk},r}$ are reduced as a result of nutrient limitation. The effect of nutrient limitation can counteract that of $\varepsilon(T)$ (when $E_\varepsilon > 0$), or compound it (when $E_\varepsilon < 0$). The parameterisation used here is arbitrary (Fig. S1); however, as long as $E_K > 0$ (Section S1.3), the qualitative impact of nutrient limitation is expected to remain.

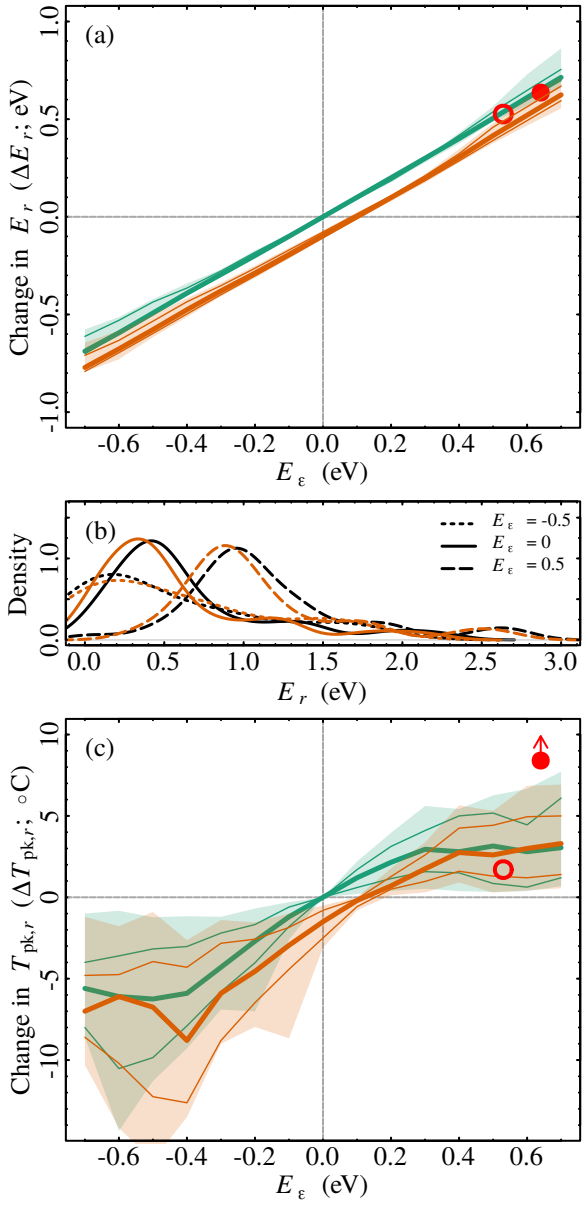

Figure S14: As in Fig. S8, but including results for nutrient limitation (shown as orange lines and shaded areas). We parameterise K_S as in Fig. S1, and use an arbitrary nutrient concentration of 1 µmol/L (Eq. S4).

S12.5 Comparing distributions of activation energies of potential and real growth rates

We put forward a hypothesis as to what values of E_ε might produce distributions of activation energies (across species) that are most consistent with distributions of activation energies estimated from actual growth rate TPCs, measured in laboratory experiments on phytoplanton. We do so by comparing distributions of activation energies of potential growth rates (estimated using TPCs of P, R, and $\varepsilon(T)$), with a distribution of activation energies estimated from actual growth rate TPCs (orange line in Fig. 4b in the main text; also see Materials and Methods). We generated a range of distributions of activation energies from potential growth rate TPCs by varying E_ε, and quantified the differences relative to a reference distribution of 'real' activation energies using the two-sample Kolmogorov-Smirnov statistic D. The patterns of Fig. S15 suggest that allocation efficiency TPCs that increase with temperature (E_ε of around 0.4 and 0.5 eV) are most likely to produce distributions that are consistent with those measured on real growth rate TPCs. However, we acknowledge that this result should be interpreted with caution; we compare distributions with different numbers of samples and from different species (potential growth rates include terrestrial and aquatic species, and the latter include macrophytes, while real growth rates only include phytoplankton). Furthermore, the distribution of activation energies from real growth rates likely includes a range of different temperature dependences of $\varepsilon(T)$.

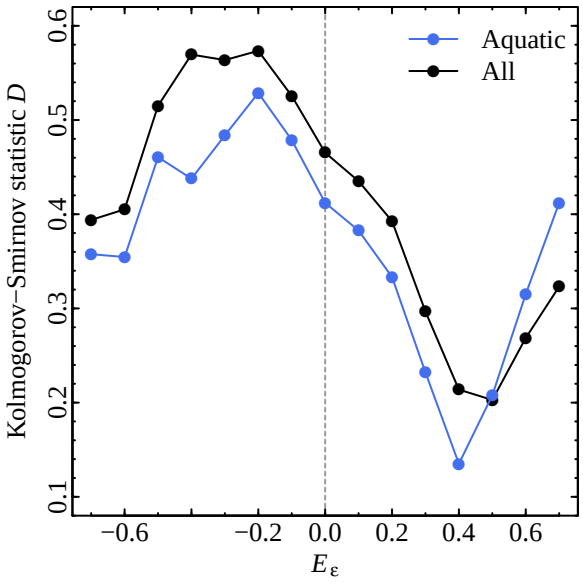

Figure S15: Comparison of the distributions activation energies of potential growth rates, and distributions of activation energies of real growth rate TPCs. The difference between the two distributions is estimated using a two-sample Kolmogorov-Smirnov statistic D, where smaller values of D indicate greater similarity between the two distributions. The distribution of activation energies of real growth rates remains the same in each test; the distribution of activation energies of potential growth rates changes with E_ε. For example, for the blue line at $E_\varepsilon = 0.5$, the comparison is between the orange and the dashed lines of Fig. 4b in the main text. Note that for the lower values of E_ε, the sample size of potential growth rate activation energies is smaller because we excluded TPCs that only decreased with temperature.

References

[1] Tilman D (1977) Resource competition between planktonic algae: an experimental and theoretical approach. *Ecology* 58:338–348.

[2] Tilman D, Mattson M, Langer S (1981) Competition and nutrient kinetics along a temperature gradient: An experimental test of a mechanistic approach to niche theory. *Limnol. Oceanogr.* 26(6):1020–1033.

[3] Reuman DC, Holt RD, Yvon-Durocher G (2014) A metabolic perspective on competition and body size reductions with warming. *J. Anim. Ecol.* 83(1):59–69.

[4] Sharpe PJH, DeMichele DW (1977) Reaction kinetics of poikilotherm development. *J. Theor. Biol.* 64:649–670.

[5] Schoolfield RM, Sharpe PJH, Magnuson CE (1981) Non-linear regression of biological temperature-dependent rate models based on absolute reaction-rate theory. *J. Theor. Biol.* 88:719–731.

[6] Padfield D, Yvon-Durocher G, Buckling A, Jennings S, Yvon-Durocher G (2016) Rapid evolution of metabolic traits explains thermal adaptation in phytoplankton. *Ecol. Lett.* 19:133–142.

[7] Schaum CE, et al. (2017) Adaptation of phytoplankton to a decade of experimental warming linked to increased photosynthesis. *Nature Ecol. Evol.* 1:0094.

[8] Kontopoulos DG, García-Carreras B, Sal S, Smith TP, Pawar S (2018) Use and misuse of temperature normalisation in meta-analyses of thermal responses of biological traits. *PeerJ* p. 6:e4363.

[9] Allen AP, Gillooly JF, Brown JH (2005) Linking the global carbon cycle to individual metabolism. *Funct. Ecol.* 19:202–213.

[10] López-Urrutia Á, San Martin E, Harris RP, Irigoien X (2006) The metabolic balance of the oceans. *P. Natl. Acad. Sci. USA* 103(23):8739–8744.

[11] Allison SD (2014) Modeling adaptation of carbon use efficiency in microbial communities. *Front. Microbiol.* 5:571.

[12] Droop MR (1973) Some thoughts on nutrient limitation in algae. *J. Phycol.* 9:264–272.

[13] Geider RJ, MacIntyre HL, Kana TM (1997) Dynamic model of phytoplankton growth and acclimation: responses of the balanced growth rate and the chlorophyll a-carbon ratio to light, nutrient-limitation and temperature. *Mar. Ecol. Prog. Ser.* 148:187–200.

[14] Geider RJ, MacIntyre HL, Kana TM (1998) A dynamic regulatory model of phytoplanktonic acclimation to light, nutrients, and temperature. *Limnol. Oceanogr.* 43(4):679–694.

[15] Baird ME, Emsley SM, McGlade JM (2001) Modelling the interacting effects of nutrient uptake, light capture and temperature on phytoplankton growth. *J. Plankton Res.* 23(8):829–840.

[16] Follows MJ, Dutkiewicz S, Grant S, Chisholm SW (2007) Emergent biogeography of microbial communities in a model ocean. *Science* 315(5820):1843–1846.

[17] Dell AI, Pawar S, Savage VM (2011) Systematic variation in the temperature dependence of physiological and ecological traits. *P. Natl. Acad. Sci. USA* 108(26):10591–10596.

[18] Dell AI, Pawar S, Savage VM (2014) Temperature dependence of trophic interactions are driven by asymmetry of species responses and foraging strategy. *J. Anim. Ecol.* 83:70–84.

[19] Lang, Birgit ERB, Ulrich B, Rall BC (2017) Temperature and consuer type dependencies of energy flows in natural communities. *Oikos* 126(12):1717–1725.

[20] Peters RH (1983) *The Ecological Implications of Body Size.* (Cambridge University Press, Cambridge, UK).

[21] Del Giorgio PA, Cole JJ (1998) Bacterial growth efficiency in natural aquatic systems. *Ann. Rev. Ecol. Syst.* 29:503–541.

[22] Gifford RM (2003) Plant respiration in productivity models: conceptualisation, representation and issues for global terrestrial carbon-cycle research. *Func. Plant Biol.* 30:171–186.

[23] Brown JH, Gillooly JF, Allen AP, Savage VM, West GB (2004) Toward a metabolic theory of ecology. *Ecology* 85(7):1771–1789.

[24] Vasseur DA, McCann KS (2005) A mechanistic approach for modeling temperature-dependent consumer-resource dynamics. *Am. Nat.* 166(2):184–198.

[25] Fogg GE, Nalewajko C, Watt WD (1965) Extracellular products of phytoplankton photosynthesis. *Proc. R. Soc. B* 162(989):517–534.

[26] Baines SB, Pace ML (1991) The production of dissolved organic matter by phytoplankton and its importance to bacteria: Patterns across marine and freshwater species. *Limnol. Oceanogr.* 36(6):1078–1090.

[27] Alldredge AL, Passow U, Logan BE (1993) The abundance and significance of a class of large, transparent organic particles in the ocean. *Deep-Sea Res. I* 40(6):1131–1140.

[28] Engel A (2002) Direct relationship between CO_2 uptake and transparent exopolymer particles production in natural phytoplankton. *J. Plankton Res.* 24(1):49–53.

[29] Engel A, Thoms S, Riebesell U, Rochelle-Newall E, Zondervan I (2004) Polysaccharide aggregation as a potential sink of marine dissolved organic carbon. *Nature* 428(6986):929–932.

[30] Riebesell U (2004) Effects of CO_2 enrichment on marine phytoplankton. *J. Oceanogr.* 60(4):719–729.

[31] Carlson CA, Hansell DA (2015) *Biogeochemistry of Marine Dissolved Organic Matter*, eds. Hansell DA, Carlson CA. (London, UK), pp. 65–126.

[32] Larsson U, Hagström A (1979) Phytoplankton exudate release as an energy source for the growth of pelagic bacteria. *Mar. Biol.* 52(3):199–206.

[33] Amthor JS (1994) *Physiology and Determination of Crop Yield*, eds. Boote KJ, Bennett JM, Sinclair TR, Paulsen GM. (American Society of Agronomy, Madison, WI), pp. 221–250.

[34] Amthor JS (1995) Terrestrial higher-plant response to increasing atmospheric [CO_2] in relation to the global carbon cycle. *Glob. Change Biol.* 1:243–274.

[35] Aksnes DL, Egge JK (1991) A theoretical model for nutrient uptake in phytoplankton. *Mar. Ecol. Prog. Ser.* 70:65–72.

[36] Smith NG, Dukes JS (2013) Plant respiration and photosynthesis in global-scale models: incorporating acclimation to temperature and CO_2. *Glob. Change Biol.* 19:45–63.

[37] Atkin OK, Bruhn D, Hurry VM, Tjoelker MG (2005) The hot and the cold: unravelling the variable response of plant respiration to temperature. *Func. Plant Biol.* 32:87–105.

[38] Amthor JS (1984) The role of maintenance respiration in plant growth. *Plant Cell Environ.* 7:561–569.

[39] Thomas MK, et al. (2017) Temperature-nutrient interactions exacerbate sensitivity to warming in phytoplankton. *Glob. Change Biol.* 23(8):3269–3280.

[40] Thornley JHM (1970) Respiration, growth and maintenance in plants. *Nature* 227:304–305.

[41] Raven JA, Geider RJ (1988) Temperature and algal growth. *New Phytol.* 110:441–461.

[42] Pasciak WJ, Gavis J (1976) Transport limitation of nutrient uptake in phytoplankton. *Limnol. Oceanogr.* 19(6):881–888.

[43] Shimeta J, Jumars PA (1991) Physical mechanisms and rates of particle capture by suspension-feeders. *Oceanogr. Mar. Biol. Annu. Rev.* 29:191–257.

[44] Armstrong RA (2008) Nutrient uptake rate as a function of cell size and surface transporter density: A michaelis-like approximation to the model of pasciak and gavis. *Deep-Sea Res. I* 55:1311–1317.

[45] Bonachela JA, Michael R, Levin SA (2011) Dynamic model of flexible phytoplankton nutrient uptake. *P. Natl. Acad. Sci. USA* 108(51):20633–20638.

[46] Sommer U (1996) Plankton ecology: The past two decades of progress. *Naturwissenschaften* 83:293–301.

[47] Raven JA (1982) The energetics of freshwater algae; energy requirements for biosynthesis and volume regulation. *New Phytol.* 92:1–20.

[48] Huey RB, Stevenson RD (1979) Integrating thermal physiology and ecology of ectotherms: a discussion of approaches. *Am. Zool.* 19(1):357–366.

[49] Huey RB, et al. (2012) Predicting organismal vulnerability to climate warming: roles of behaviour, physiology and adaptation. *Phil. Trans. R. Soc. B* 367:1665–1679.

[50] Savage VM, Gillooly JF, Brown JH, West GB, Charnov EL (2004) Effects of body size and temperature on population growth. *Am. Nat.* 163(3):429–441.

[51] Rall BC, Vucic-Pestic O, Ehnes RB, Emmerson M, Brose U (2010) Temperature, predator–prey interaction strength and population stability. *Glob. Change Biol.* 16:2145–2157.

[52] Thomas MK, Kremer CT, Klausmeier CA, Litchman E (2012) A global pattern of thermal adaptation in marine phytoplankton. *Science* 338(6110):1085–1088.

[53] Sal S, Alonso-Sáez L, Bueno J, García FC, López-Urrutia Á (2015) Thermal adaptation, phylogeny, and the unimodal size scaling of marine phytoplankton growth. *Limnol. Oceanogr.* 60(4):1212–1221.

[54] Pawar S, Dell AI, Savage VM, Knies JI (2016) Real versus artificial variation in the thermal sensitivity of biological traits. *Am. Nat.* 187(2):E41–E52.

[55] Ruel JJ, Ayres MP (1999) Jensen's inequality predicts effects of environmental variation. *Trends Ecol. Evol.* 14(9):361–366.

[56] Martin TL, Huey RB (2008) Why "suboptimal" is optimal: Jensen's inequality and ectotherm thermal performance. *Am. Nat.* 171(3):E102–E118.

[57] García-Carreras B, Reuman DC (2013) Are changes in the mean or variability of climate signals more important for long-term stochastic growth rate? *PLOS One* 8(5):e63974.